NASA SP-8010

NASA SPACE VEHICLE DESIGN CRITERIA (ENVIRONMENT)

MODELS OF MARS' ATMOSPHERE [1974]

REVISED
DECEMBER 1974

NATIONAL AERONAUTICS AND SPACE ADMINISTRATION

FOREWORD

NASA experience has indicated a need for uniform criteria for the design of space vehicles. Accordingly, criteria have been developed in the following areas of technology:

Environment
Structures
Guidance and Control
Chemical Propulsion

Individual components of this work are issued as separate monographs as soon as they are completed. A list of all monographs published in this series can be found on the last pages of this monograph.

These monographs are to be regarded as guides to design and not as NASA requirements, except as may be specified in formal project specifications. It is expected, however, that the monographs will be used to develop requirements for specific projects and be cited as the applicable documents in mission studies, or in contracts for the design and development of space vehicle systems.

This monograph was prepared for NASA under the cognizance of the NASA Goddard Space Flight Center with Scott A. Mills as program coordinator. Principal authors were Richard B. Noll of Aerospace Systems, Inc. and Dr. Michael B. McElroy of Harvard University. The Technical Director was Mr. John Zvara of Aerospace Systems, Inc. This monograph is based on a draft manuscript prepared by Y. S. Lou of Northrop Services, Inc. His efforts which are included in part are gratefully acknowledged.

Comments concerning the technical content of these monographs will be welcomed by the National Aeronautics and Space Administration, Goddard Space Flight Center, Systems Reliability Directorate, Greenbelt, Maryland 20771.

December 1974

CONTENTS

MODELS OF MARS' ATMOSPHERE [1974]

1. INTRODUCTION

The purpose of this monograph is to provide atmospheric models for support of design and mission planning of space vehicles that are to orbit the planet Mars, enter its atmosphere, or land on the surface. The atmosphere affects the orbital lifetime, the flight dynamics of the vehicle along its flight path, and the performance of the vehicle and its major subsystems. For design of experiments, knowledge of the Martian atmosphere is required to select instrumentation and establish the range of measurements.

Quantitative data for the Martian atmosphere have been obtained from Earth-based observations and from spacecraft that have orbited Mars or passed within several planetary radii. These data have been used in conjunction with existing theories of planetary atmospheres to predict other characteristics of the Martian atmosphere as discussed in reference 1. Because of limited observational data, it was necessary to extrapolate within the limits of applicable theory to establish reasonably complete model atmospheres. Earth-based observations have generally provided information on the composition, temperature, and optical properties of Mars with rather coarse spatial resolution, whereas spacecraft measurements have yielded data on composition, temperature, pressure, density, and atmospheric structure with moderately good spatial resolution.

The models herein provide the temperature, pressure, and density profiles required to perform basic aerodynamic analyses. The profiles are supplemented by computed values of viscosity, specific heat, and speed of sound. These ambient values and the calculated aerodynamic forces influence flight dynamics and space vehicle design; i.e., configuration, size, strength, and materials. Other characteristics are inferred from the measured data that also affect design. For example, electron densities of the ionosphere and the plasma characteristics in the region of the solar wind may dictate requirements for electromagnetic shielding. Also, opacity of the atmosphere caused by dust storms could constrain the design of landed solar power systems and may adversely affect performance of experiments.

This monograph provides a set of engineering models for the Martian atmosphere on the basis of theory and measured data available in July 1974. It replaces NASA SP-8010 of May 1968 (ref. 2). Data from US and USSR space exploration have narrowed considerably the range of parameters in the lower atmosphere in comparison to the 1968 monograph. The four model atmospheres developed herein include a model for a dusty atmosphere, a nominal model for a clear atmosphere, and two other models that encompass reasonable extremes of exospheric temperature.

Design criteria monographs on other planets, Earth environments, and space technology are listed in the last pages of this monograph.

2. STATE OF THE ART

The need for information on the Martian atmosphere that could be used to develop atmospheric engineering models for spacecraft design purposes was recognized in the middle 1960s (e.g., refs. 3, 4, and 5). Continuous observation of Mars from Earth, particularly by radio and radar astronomy, and the successful flyby mission of Mariner 4 in 1965 provided new information which was incorporated into improved models such as presented in reference 2. Since the publication of reference 2, knowledge of the Martian atmosphere and of the planet itself has undergone many changes. The most significant information came from the Mariner 6, 7, and 9 experiments. The revised Mars engineering models for the Viking Project (ref. 6) were developed on the basis of new findings from Mariner 6 and 7 missions.

Although the Mariner 9 mission did not provide in-situ measurements of the Martian atmosphere such as obtained from Venus spacecraft missions (ref. 7), the spacecraft was placed in orbit around Mars on November 14, 1971 and provided a remarkably successful record of planetary conditions over a moderately long time base. Multispectral sensing devices were used to observe Mars on a global basis and permitted a determination of atmospheric characteristics as a function of spatial position, local time, and season. As a result, it is now possible to reduce significantly the uncertainties inherent in spatially- and time-averaged models.

2.1 Atmosphere

For discussion of engineering models, the Martian atmosphere is divided into lower and upper regions as shown in figure 1. Reference 8 provides an overview of the impact of Mariner 9 on the knowledge of Mars as well as a useful reference chart. Reference 9 gives a more detailed account. The following sections briefly describe the current status of information for the parameters needed to construct model atmospheres.

2.1.1 Lower Atmosphere

2.1.1.1 Surface Pressure

Modern studies of the Martian atmospheric pressure began in 1963 with the spectroscopic study of Kaplan, Munch, and Spinrad (ref. 10). Subsequent spectroscopic results were reported in references 11 through 15. Of particular interest is the work by Grandjean and Goody (ref. 15) who used the observation of carbon dioxide (CO_2) to determine the relationship between the surface pressure and the total volume fraction of CO_2. The full significance of this result was not appreciated because of the then prevailing theories that favored high values for atmospheric pressure. Goody (ref. 16) noted that the assumption of a pure CO_2 atmosphere led to a lower limit for the surface pressure of 13 mb. Another analysis made by Belton and Hunten (ref. 12) gave 5.5 ± 0.5 mb. Low pressure was also derived by Musman (ref. 17) and Evans (ref. 18) from Martian ultraviolet albedos. Musman used an albedo for the total disc obtained photoelectrically by de Vaucouleurs (ref. 19). With assumptions of no absorbing atmospheric constituents, no particles in the atmosphere

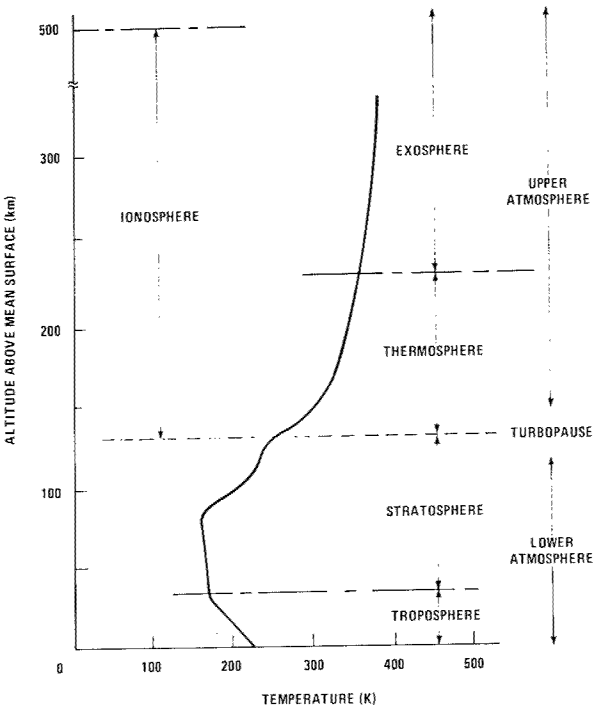

Figure 1.—Atmospheric Regions of Mars.

that might contribute to the albedo, and a surface reflectivity of zero, Musman calculated a surface pressure of 27 mb for a pure N_2 atmosphere and 19 mb for a pure CO_2 atmosphere. On the other hand, Evans found surface pressures of 6 ± 3 mb for pure CO_2, 9 ± 4 mb for pure nitrogen (N_2), and 12 ± 6 mb for pure argon (A) atmospheres on the basis of an ultraviolet spectrum from 2400 to 3600 Å that was obtained by an Aerobee rocket.

Through a careful examination of spectroscopic measurements, Wood (ref. 20) concluded that the values of the surface pressure on Mars fall between 5 and 7 mb except for two measurements which yielded pressures of 4.4 mb and 8.0 mb. Wood derived a mean Martian surface pressure of 5.3 mb on the basis of spectroscopic measurements of CO_2 abundance.

Additional information on the atmospheric pressure was obtained from Mariner 4, 6, and 7 occultation experiments in which changes in the frequency, phase, and amplitude of the S-band radio signal during passage through the atmosphere of Mars, were observed immediately before and after occultation by the planet. Analysis of these effects yielded estimates of the refractivity and density of the atmosphere near the surface, the scale height in the atmosphere, and the electron density profile of the ionosphere. From these data, surface pressure was estimated in the 4.2 to 8.0 mb range (refs. 21 through 26).

The most recent results for surface pressure were derived from both ground-based observations and Mariner 9 experiments. Absorption of CO_2 in the Martian atmosphere (from which the partial pressure of CO_2 can be inferred) was measured from Earth by means of a multislit spectrometer in 1969 (ref. 27) and in 1971 (ref. 28). These measurements, which

provided moderate spatial resolution, covered about three-fourths of the circumference from 40° N to 20° S latitude in 1969 and almost all of the surface from 40° N to 60° S in 1971. The results of these measurements were in general agreement.

An occultation experiment similar to those of Mariner 4, 6, and 7 was conducted on Mariner 9 (ref. 29). The results were similar to the previous occultation results even though the measurements were made at a time when the entire planet was shrouded by a dust storm. This storm obscured the surface at wavelengths ranging from the ultraviolet to the infrared (ref. 30). Unlike earlier Mariners, Mariner 9 was placed in orbit around Mars so it provided occultation measurements over various regions. Measurements made in the equatorial regions resulted in an average surface pressure of about 4.95 mb without taking into account minimum and maximum measurements. The minimum surface pressure of approximately 2.8 mb was measured in the Phoenicis Lacus region of the Tharsis ridge area as well as in the Claritas area at approximately 34.5° S latitude. The highest surface pressure of 8.9 mb was measured at the bottom of the Hellas depression.

Surface pressures at about 65° N latitude were considerably higher than those in the equatorial region. Pressures ranged from about 7.2 to 10.3 mb with a mean value of approximately 8.9 mb. The pressures derived from Mariner 9 occultation data are in agreement with Earth-based spectroscopic results of reference 28.

The difference in surface pressures shown by the spectroscopic and occultation results correlates with the topography of Mars.* Radar observations and spacecraft occultation experiments prior to 1969 showed that the elevation difference on Mars was about 12 km (refs. 31 through 34). References 35, 36, and 37 indicated elevation variations of about 14 km. However, recent topographic estimates that have been derived from occultation, radar, spectral, and optical measurements show a range of elevations from 4 km below the mean surface in Hellas depression to an altitude of 28 km on Olympus Mons as shown in figure 2.**

The surface pressure data achieved by the Mariner 9 occultation experiment strongly suggest that the physical shape of Mars is substantially more oblate that its gravitational equipotential surface and is approximated by a triaxial ellipsoid (ref. 38). Optical measurements of Mars indicate that the shape is an ellipsoid with an equatorial radius of 3398 ± 3 km and a polar radius of 3371 ± 4 km (ref. 39). Earth and Mariner 9 observations were combined to yield ellipsoid radii of 3400.12, 3394.19, and 3375.45 km.*** The mean equatorial radius of Mars determined from combined radar data is 3394 ± 2 km (ref. 36).

*Besides variation with topography, seasonal variation of surface pressure by 10 to 20 percent is indicated in recent study by P. M. Woiceshyn, "Global Seasonal Fluctuations on Mars," Icarus 22, July 1974.

**I. J. Christensen, "Martian Topography Derived from Occultation, Radar, Spectral and Optical Measurements," Journal of Geophysical Research, to be published in early 1975.

***D. L. Cain et al., "Approximations to the Mean Surface of Mars and Mars Atmosphere Using Mariner 9 Occultations," Chapter 37 of Mariner Mars 1971 Project Final Report, vol. IV (ref. 9), July 15, 1973, pp. 495-498.

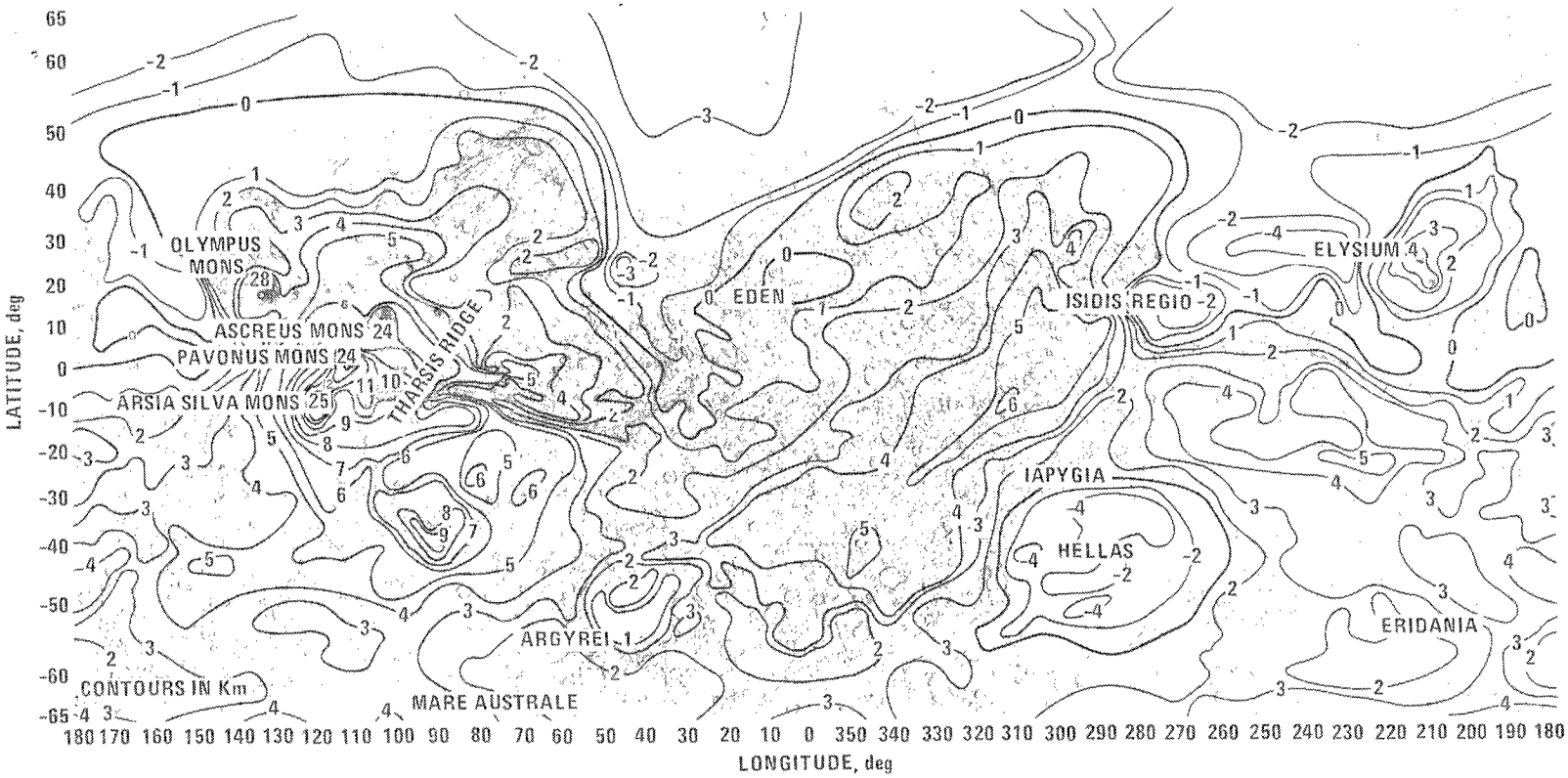

Figure 2. — Topographic Map of Mars (Altitudes in km).

Table 1
Composition of the Martian Atmosphere
(ref. 40)

Constituent	Abundance (cm atm)*
CO_2	7800
CO	5.6
O_2	10.4
H_2O	~ 3, variable
H_2	~ 0.4
O_3	$\sim 10^{-4}$
N_2	<400
A + inert gases	<1560
SO_2	$<3 \times 10^{-3}$
N_2O	<200
CH_4	<10
C_2H_4	<2
C_2H_6	<1
NH_3	<2
NO_2	$<8 \times 10^{-4}$

*These values give the abundance of each gas according to its thickness in cm if spread evenly over the planet. The uniform density is that for standard temperature and pressure (0° C and 760 mm Hg). 1 cm atm is equivalent to a 1 cm thickness and contains 2.69×10^{23} molecules/m^2.

2.1.1.2 Composition and Molecular Mass

Present knowledge of the composition of the Martian atmosphere is based on spectroscopic observations and on theoretical deductions that certain gases are present. Additionally, the polarization and occultation measurements provide information on the total amount of gases. Table 1 from reference 40 lists the abundances of all the observed and assumed constituents.

A. Major Constituents

Of the expected major constituents (N_2, CO_2, and A), only CO_2 has been observed spectroscopically. The amount of CO_2 reported lies within the range of 50 to 90m-atm (refs. 10, 12, 41 through 46), and the arithmetic mean of CO_2 abundance for the ten best measurements was 72 m-atm (ref. 6). A current value is 78m-atm (ref. 40). On the basis of the observed spatial variations of total pressure, one would expect similar spatial variations for CO_2.

A small amount of nitrogen may be present in the Martian atmosphere even though it was not detected by the ultraviolet spectrometers on the Mariner 6, 7, and 9 spacecraft. From Mariner 6 and 7 evidence that the ionosphere of Mars contains CO_2^+ ions, Goody (ref. 47)

noted that the amount of nitrogen present in the Martian atmosphere must be less than ten percent or else the ions would be OH^+ and CO^+. Dalgarno and McElroy (ref. 48) estimated the maximum mole fraction of N_2 relative to CO_2 must be less than five percent on the basis of an analysis of dayglow data. It has been suggested (ref. 6) that the presence of one percent nitrogen may be assumed for the purpose of calculating radio blackout phenomena.

The possibility of potassium compounds near the surface of Mars led to the long-held assumption that the Martian atmosphere contains some argon associated with the production of potassium 40 by radioactive decay. The amount of argon in the Martian atmosphere is probably small. Recent studies (refs. 25 and 49 through 52) all confirm that CO_2 is the only major constituent; inert species other than argon can account for at most ten percent of the total atmospheric mass.*

B. Minor Constituents

Besides water vapor and dust, minor identified constituents are CO, O_2, and O_3. Water vapor was first detected spectroscopically by Spinrad, Munch, and Kaplan (ref. 53). An analysis of the line intensities gave an average abundance of 14 ± 7 μm precipitable water over the entire planet. Other findings for H_2O were reported by Dollfus (ref. 54) who gave value of 45 μm precipitable water, the highest determination, and by Schorn et al. (ref. 55) who estimated an abundance of 10 to 20 μm precipitable water from study of the lines of H_2O near 8200Å with a new high-dispersion spectrograph during the 1964-65 apparition. The mean relative humidity of the Martian atmosphere may be as high as 50 percent (ref. 56).

Seasonal and latitudinal variations of water vapor content have been reported by Tull (ref. 57) who found that during the period from the middle summer to the middle autumn the amount of precipitable water vapor reached as much as 48 μm in the northern hemisphere and 20 μm in the southern hemisphere. Schorn et al. (ref. 56) reported that more precipitable water vapor was found in the northern hemisphere in the northern midspring and more in the southern hemisphere in the northern midsummer.

Water vapor was identified conclusively from spectra obtained by the infrared interferometer spectroscopy (IRIS) experiment on Mariner 9 (ref. 37). The total H_2O content was determined from a quantitative comparison of observed and synthesized spectra. This comparison indicated the abundance of water vapor at 10 to 20 μm of precipitable water. Water vapor data from the IRIS experiment are compared to Earth-based observations (refs. 58 and 59) in figure 3. The data shown by the dashed lines were made concurrently with the IRIS data. Latitudinal gradients were not found to be significant from the South pole to the equator. The 1971 Earth-based measurements and IRIS data are in general agreement; however, Earth measurements in previous years during similar seasonal conditions indicated larger amounts of water vapor. Results from the 1.38 μm water vapor band experiment on the USSR Mars 3 indicate substantially lower water vapor amounts (ref. 60) although the reason for an actual discrepancy is not clear.

*Reported detection of considerable amounts of an inert atmospheric gas by the recent Soviet lander is discussed by G. P. Wood in NASA TM X-71999, August 1974.

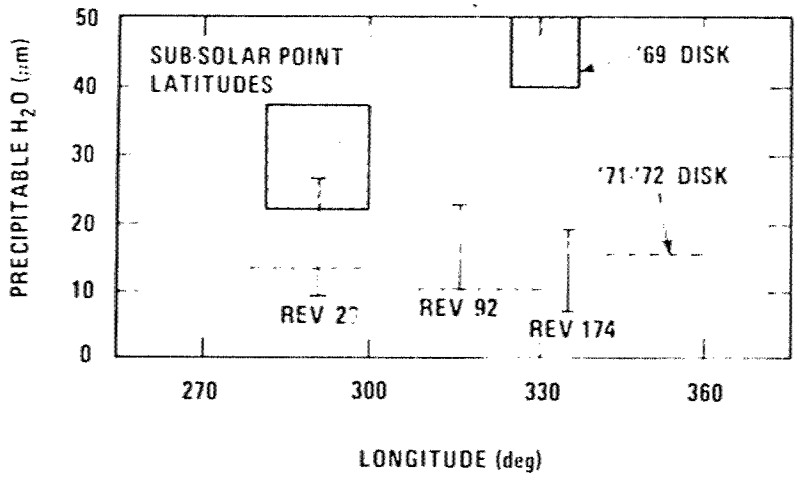

a. South Sub-Solar Point Latitudes (20 to 30 S)

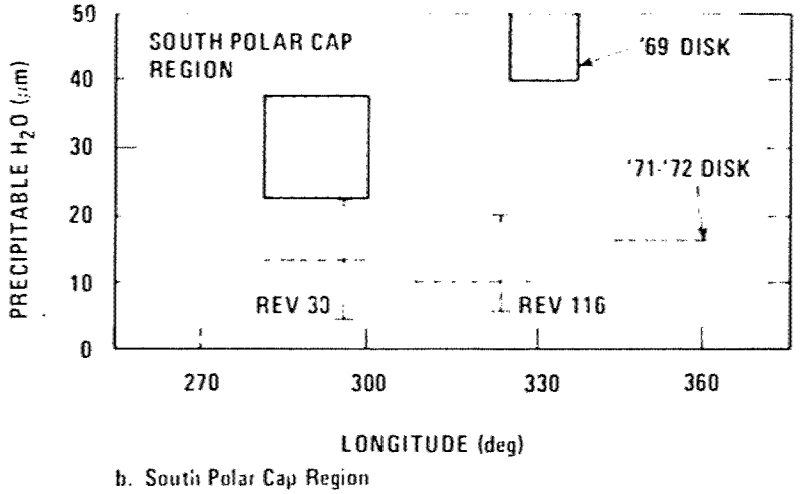

b. South Polar Cap Region

BARKER ET AL. (REF. 58)

TULL & BARKER (REF. 59)

MARINER 9 (REF. 37)

Figure 3.—Water Vapor Content of the Martian Atmosphere (ref. 37).

The average abundance of water vapor determined by IRIS was lower than values observed during previous oppositions. It is theorized that this could result from an unusually large amount of water trapped in the north polar cap (water vapor was not detected over the north polar hood) or that the large dust storm in late 1971 could have resulted in the adsorption of water vapor on the dust particles.

When Mariner 9 entered into orbit of Mars on November 14, 1971, the entire planet was shrouded by a dust storm. Thus, dust must be considered as a likely atmospheric constituent. Comparison of Mariner 9 observations of the brightness of the dust storm with results from a simple multiple scattering theory (ref. 61) leads to an albedo of about 0.7 for the particles. This is consistent with values for Martian surface albedo obtained from Earth-based measurements. Therefore, the mean size and composition of the dust storm particles appear to be similar to those for particles on the Martian surface. The mean particle size of surface material has been estimated as 100 μm in references 62 and 63 and between 10 and 300 μm in reference 64.

Because mineralogical characteristics determine the spectral position of absorption and transmission maxima (e.g., ref. 65), it is possible to infer the dust composition from Mariner 9 IRIS results. An empirical comparison of these data with laboratory transmission spectra of mineral dust indicates a SiO_2 content of 60 ± 10 percent (ref. 37).

Other identified minor species of the lower Martian atmosphere are carbon monoxide (CO) detected by Kaplan et al. (ref. 49), oxygen (O_2) observed by Carleton and Traub (ref. 66), and ozone (O_3) measured by Lane et al. (ref. 67). Both CO and O_2 should be well mixed throughout the lower atmosphere of Mars. Their abundances are 5.6 cm-atm and 10.4 cm-atm, respectively.

Ozone was observed by the Mariner 7 ultraviolet spectrometer experiment at the Martian south polar cap during its late spring season but nowhere else (ref. 68). Results from a similar experiment on Mariner 9 (ref. 67) also indicated the presence of O_3 in the Martian atmosphere during the southern summer season. In the foregoing observations, ozone was detected only in the polar region north of 45°N, but it was subsequently detected in the southern hemisphere with the approach of the autumnal equinox. The presence of ozone appears to increase as the amount of water vapor in the atmosphere decreases (ref. 67).

There are upper limits for the abundances of formaldehyde (HCHO), carbonyl sulfide (COS), ammonia (NH_3), methane (CH_4), and oxides of nitrogen such as NO_2, N_2O_4, NO, N_2O, and HNO_2. Theoretical models (refs. 28 and 69) indicate expected densities for H_2O_2, H_2, H, OH, and HO_2 species that play a major role in the chemistry of the Martian atmosphere.

C. Molecular Mass

From Mariner 4 occultation data, Spencer (ref. 70) has shown for a mean temperature above the occultation point of 140 to 180 K, the allowable mean molecular weight could range from 33.1 to 50. Similarly, Hess and Pounder (ref. 71) indicated that although the mean molecular weight estimated from the Mariner 4 data is between 33.2 and 39.2, a range of

31.2 to 44 is consistent with reliable spectroscopic data. More recently, both Mariner 6 and 7 occultation experiments indicated that the molecular weight of the Martian atmosphere is close to 44 (refs. 23 and 24). Thus, the more recent data interpretations strongly favor a CO_2 rich atmosphere in which CO_2 accounts for at least 90 percent of the total atmospheric mass.

2.1.1.3 Temperature

Numerous theoretical models have been developed to describe the thermal structure of the Martian atmosphere (e.g., refs. 72, 73, and 74). These analyses are generally based on assumptions of radiative, convective, and conductive equilibrium for the Martian atmosphere and surface. One recent analysis (ref. 75) also includes absorption of solar energy by a grey atmosphere such as might be caused by the global dust storm of 1971. These theoretical techniques are in general accord and demonstrate variation of temperature with latitude and season.

The vertical temperature structure of Mars has been determined from occultation experiments on Mariner 4 (refs. 21, 22, 76, and 77), Mariner 6 and 7 (refs. 23 and 24), and Mariner 9 (refs. 29 and 78) and from the Mariner 9 IRIS experiment (ref. 37). Occultation results from Mariner 6 and 7 were compared to a revised model of the analysis developed by Leovy in reference 74 (ref. 79). Predictions by this model of the Martian atmospheric characteristics at the time of the Mariner 6 and 7 flybys (ref. 80) were in excellent agreement with observed data.* Mariner 9 IRIS results obtained during the global dust storm did not correlate well with the theoretical analyses for a dust-free atmosphere. However, Mariner 9 results were in reasonable agreement with the model of a dusty atmosphere presented by Gierasch and Goody (ref. 75).

The 20,000 spectra from the Mariner 9 IRIS experiment indicated temperature variations with latitude, season, local time, topography, and secular events such as the global dust storm (ref. 37). Figure 4a shows variation with latitude and local time during the dust storm at altitudes of about 10 km (2 mb pressure level of the atmosphere). For the period after the dust storm, figure 4b shows cooling of the atmosphere and shifting of the maximum temperature toward the subsolar point at the same altitudes. The isotherms were constructed from data averaged over 10 degree bands of latitude and one hour intervals in Martian local time. The diurnal variations of 15 to 30K were larger than expected from theoretical predictions.

At the surface, figure 5** shows variation of temperature with latitude and local time during and after the dust storm (ref. 37). Maximum temperatures occurred near the subsolar point at both times with little change in the maximum.

---

*Private communication from Y. S. Lou, Northrop Services, Inc., Huntsville, Alabama.

**Figure 5 refers to the temperature on the surface. There is a large temperature drop in the first meter above the surface in the warmer parts of the day. In some temperature studies, the zero point for altitude is taken at the top boundary of this thin layer.

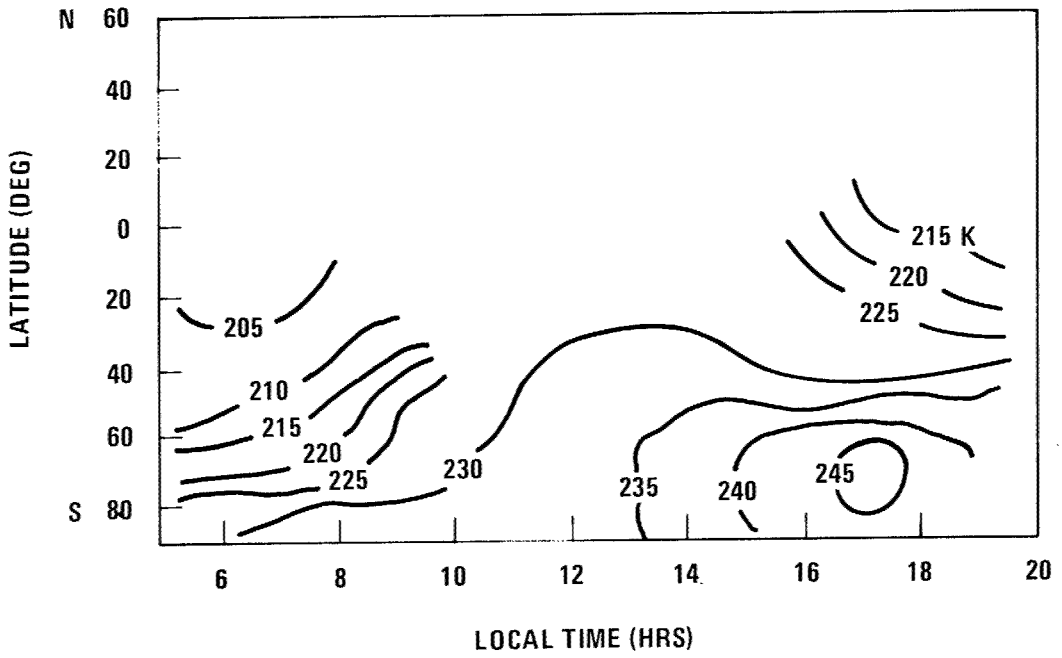

a) Revolutions 1-85 (Dust Storm)

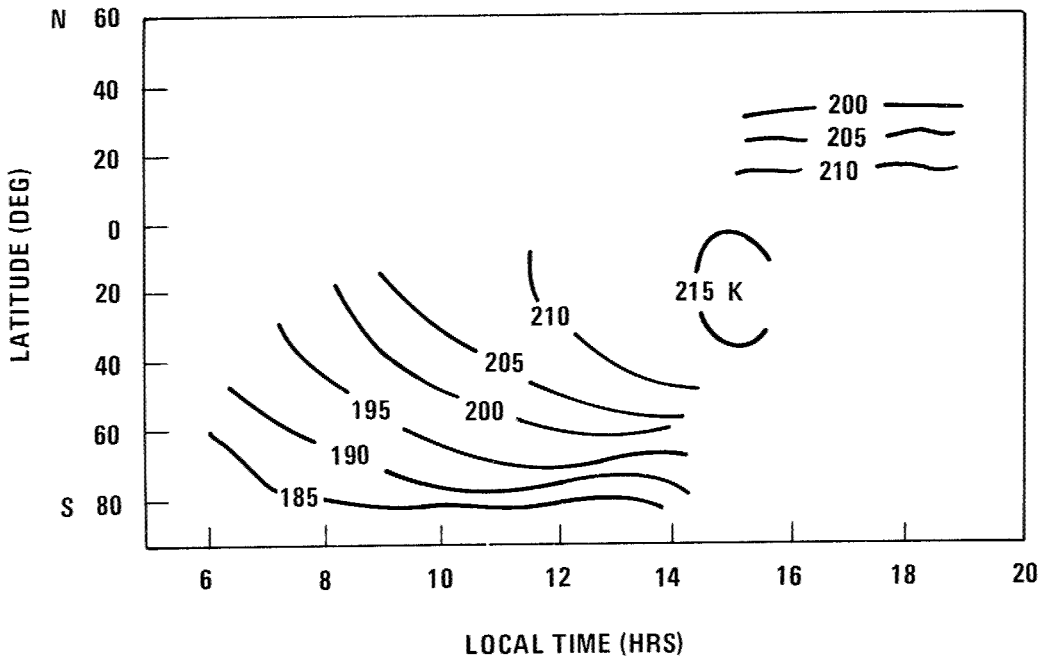

b) Revolutions 161-186 (Clearing)

Figure 4. – Variations of Atmospheric Temperature with Latitude and Local Time at Altitudes of About 10 km (2 mb Pressure Level) (ref. 37).

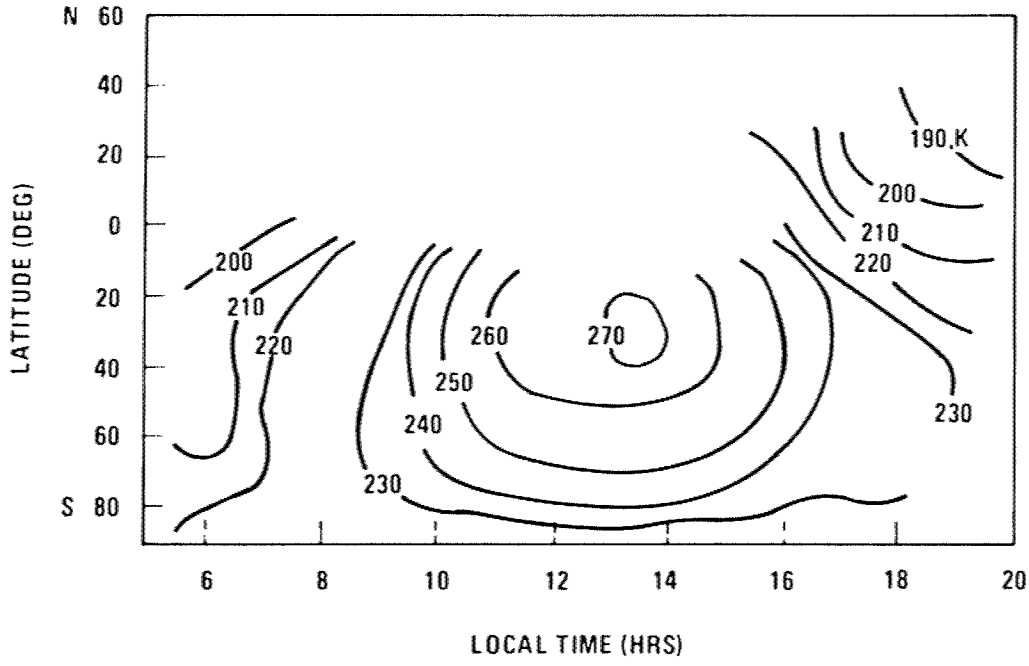

a) Revolutions 1-85 (Dust Storm)

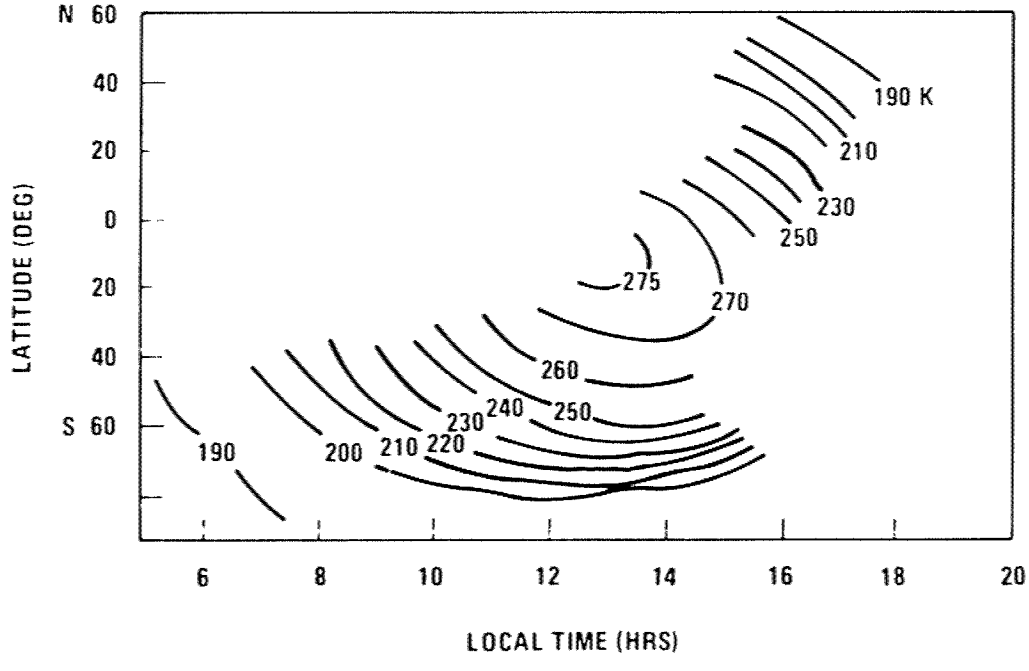

b) Revolutions 161-186 (Clearing)

Figure 5. – Variation of Surface Temperature with Latitude and Local Time (ref. 37).

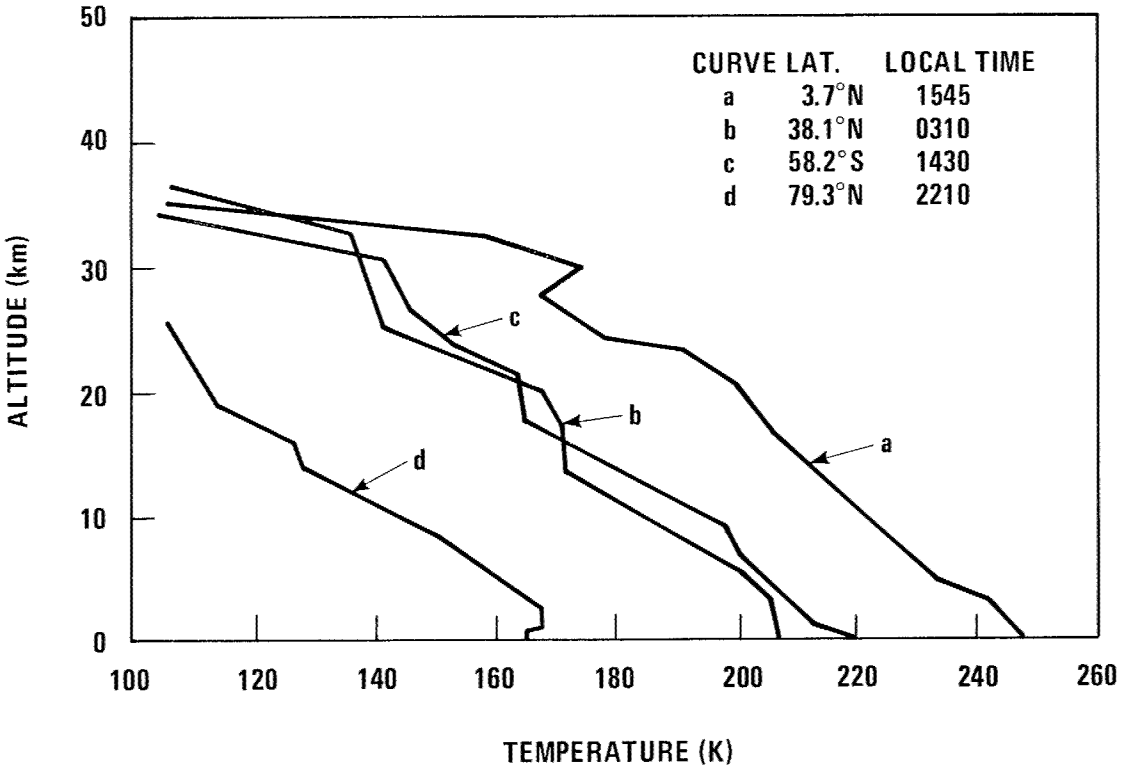

Figure 6. – Thermal Structure of Lower Martian Atmosphere – Mariner 6 and 7 Occultation Data (ref. 24).

Temperature profiles obtained from the Mariner 6 and 7 occultations are shown in figure 6 (ref. 24). The profiles are uncertain at high altitudes because of uncertainties in the motion of the spacecraft and in the refractivity of the ionosphere. These data indicate an extremely cold region in the middle atmosphere with a subadiabatic lapse rate of about 3.5 K/km. Mariner 9 occultation results reported in reference 29 were obtained during the global dust storm. Measurements at beginning of occultation were made in the equatorial region and measurements near the end at about 65°N latitude in the Martian early morning during midwinter. Therefore, the near-surface temperatures of 150 to 160 K obtained at the end of occultation were noticeably lower than at the beginning. Typical temperature profiles obtained from Mariner 9 IRIS are shown in figure 7. The cooling of the atmosphere as the dust storm diminished is evident; however, in all cases the lapse rate remained subadiabatic (ref. 37).

2.1.1.4 Winds (Atmospheric Dynamics)

Information concerning Martian winds has been obtained from observation and theory. The observational input comes largely from the study of the motion of cloud systems in the Martian atmosphere although useful information has also been derived from analysis of temperature maps made by the IRIS instrument on Mariner 9. The theoretical work is based generally on the application of standard meteorological principles (ref. 81).

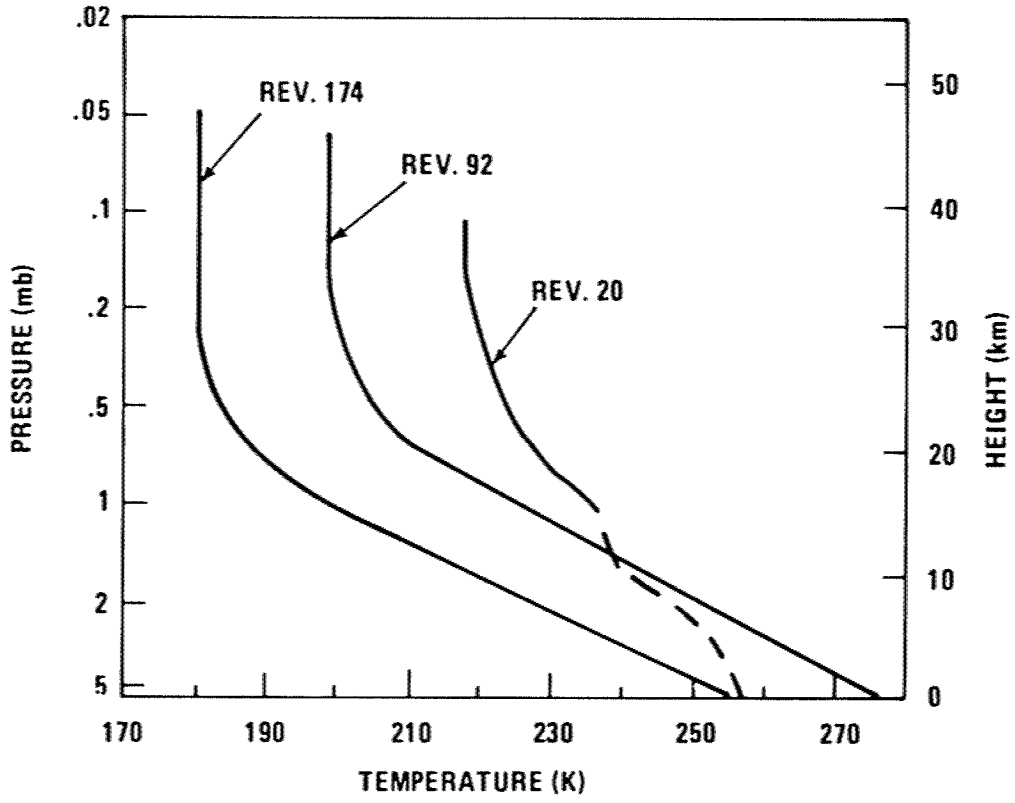

Figure 7. – Martian Temperature Profiles–Mariner 9 IRIS Data for Revolutions 20, 92, and 174 (ref. 37).

Observational studies of Martian clouds have a lengthy history. Ground based observations by Kuiper (ref. 82) and de Vaucouleurs (ref. 19) established the potential of the technique as a remote monitor of dynamic activity. They drew attention to a variety of interesting circulation phenomena. Their concepts have been followed in Mariner 9 experiments. The imaging experiment on this spacecraft provided superior spatial resolution and afforded an excellent opportunity for careful study of Martian meteorological phenomena (ref. 61).

A. Mariner 9 Results

Mariner 9 arrived at Mars during a planet-wide dust storm that altered meteorological conditions drastically. Dust was lifted to altitudes above 30 km (ref. 61). This vertical extent requires strong winds and circulation; these can be attributed to alterations in the temperature structure because of dust content. The effect of dust on heating was shown by the unexpectedly high atmospheric temperatures observed by Mariner 9 experiments. These high temperatures in conjunction with their nonuniformity in horizontal directions (refs. 37 and 75) can induce vertical circulation in two ways (ref. 61):

1) the diurnal variation of the heating can drive a large-scale circulation capable of completely overturning the atmosphere each day, and

2) if large-scale horizontal variations in dust content of the air occur, the dustier regions will be heated relative to their surroundings and will develop larger vertical velocities.

Golitsyn (ref. 83) has deduced that a dust storm can result in a cyclonic vortex with thermal winds (velocity changes) of about 40 m/s. For the upper part of the atmosphere where the temperature gradient is reversed, an anticyclonic vortex should arise. Thus, the dust storm can generate strong winds that can raise new dust from the surface. Sagan (ref. 84) concludes that wind velocities of 100 m/s and perhaps as high as 150 m/s are required to raise the dust to the observed altitude.

The effect of the large observed diurnal variations in the atmospheric temperatures during the global dust storm of 1971 on tidal winds was considered in reference 37 and extended by Pirraglia and Conrath (ref. 85). Temperature fields derived from the Mariner 9 IRIS experiment were used as input data to solve the surface pressure tidal equation and subsequently to estimate the velocities of atmospheric winds. The derived wind fields are shown in figures 8 and 9. The resulting diurnal winds near the surface beyond 30°N and S (fig. 8) have amplitudes of the order of 20 m/s. These winds could not sustain the dust storm unless augmented by the polar symmetric fields or orographic wind fields. The 70 to 100 m/s zonally-symmetric winds in the latitude belt between 30°N and 30°S could contribute to the lifting of dust into the atmosphere.

Photographs from Mariner 9 (ref. 61) also revealed local dust storms. In one case, the storms appear to be associated with a strong southward movement of cold air following a cold front at an apparent speed of 15 m/s. These highly-convective local storms carried dust as high as 15 to 20 km.

The Mariner 9 pictures also revealed a variety of additional features of the Martian meteorology. Photographs of the clouds comprising the North polar hood (north of 45°N) indicated that those clouds move in a manner that is characteristic of cold fronts and associated baroclinic wave cyclones in the Earth's atmosphere. Cloud bands were observed in the region between 45 and 65°N during the winter season. These clouds which have 30 km wavelengths are indicative of gravity waves that are generated by flow over irregular topography. Wave orientations and positions in respect to the topography show that west-to-east winds prevail in this region. Because of the static stability of the Mars atmosphere at this time (ref. 37), it was inferred that a deep layer containing westerly winds with speeds of at least 55 m/s lies above the wave-generating region (ref. 61).

B. Theoretical Studies

Information from Earth-based Martian cloud observations was used as a direct input for the theoretical study of atmospheric circulation (ref. 86) in which the presence of a wave-type circulation regime was found. A value of 100 m/s or more was obtained for the maximum surface wind and 13 m/s for the maximum large-scale vertical wind. The average zonal winds were about 25 m/s and average meridional winds about 1.3 m/s.

A comprehensive theoretical investigation of general circulation on Mars by Leovy and Mintz (ref. 87) included calculations of wind velocities for the northern vernal equinox and

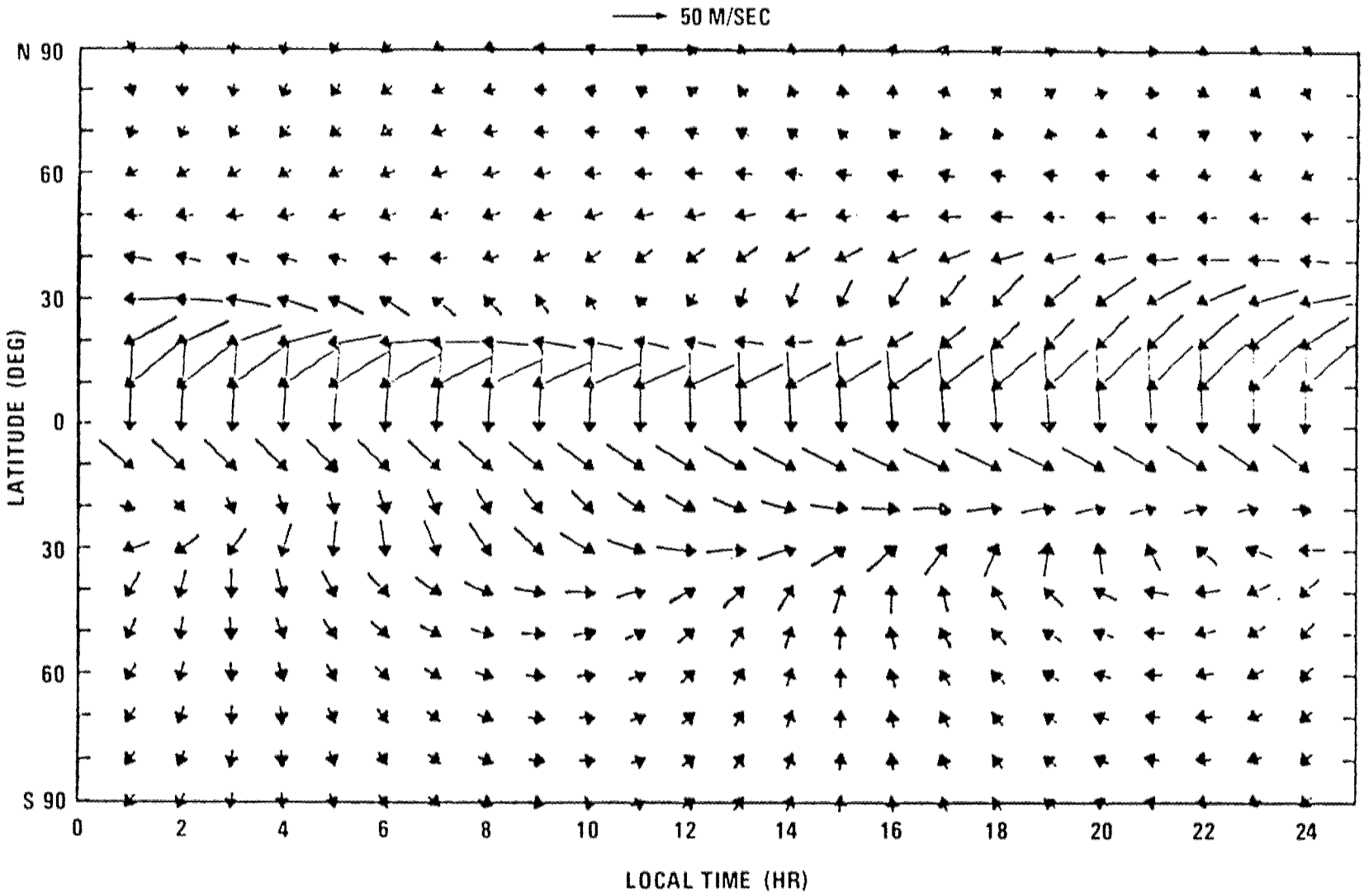

Figure 8. — Near-Surface Winds During 1971 Dust Storm (ref. 85).

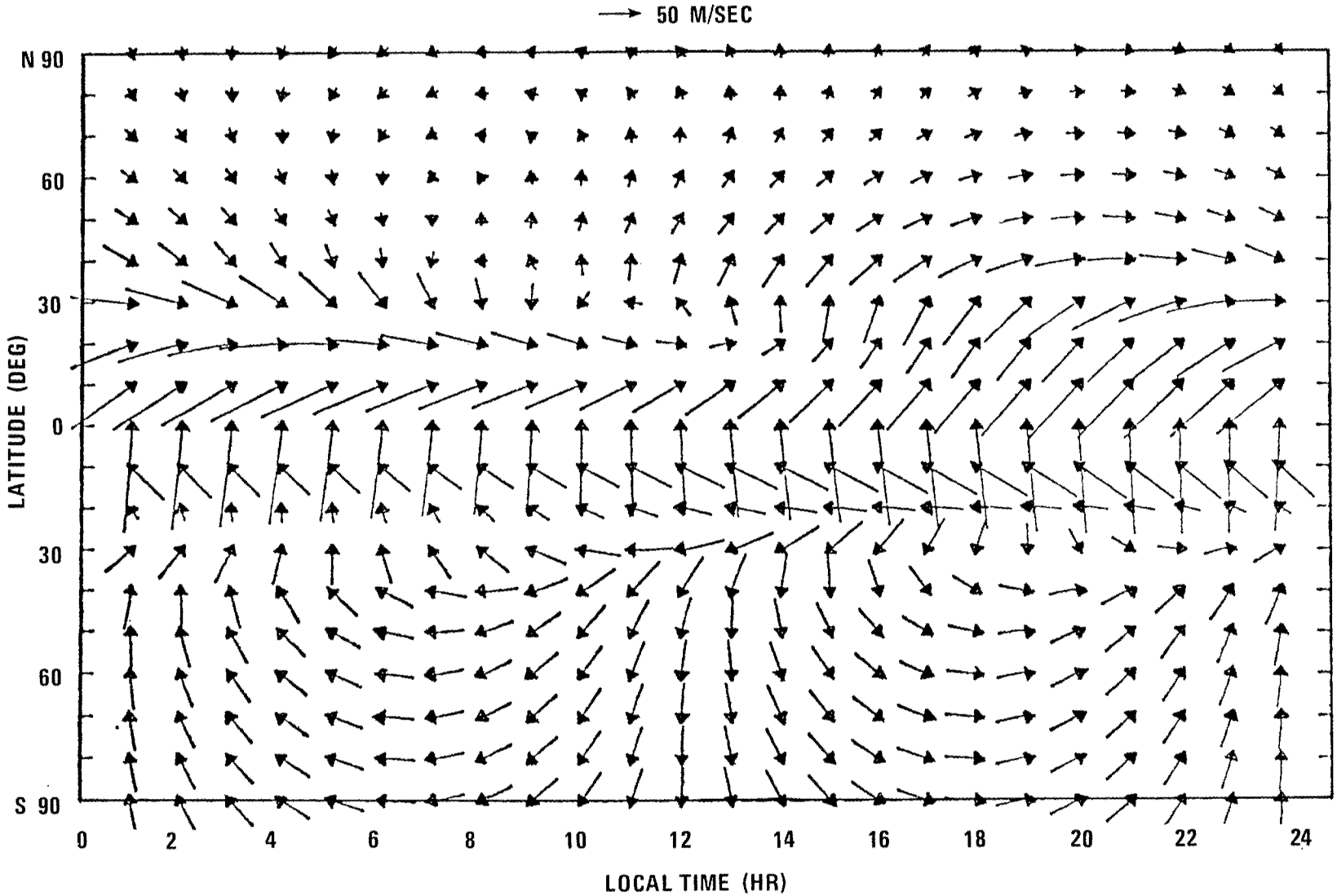

Figure 9. – High Altitude Winds During 1971 Dust Storm (ref. 85).

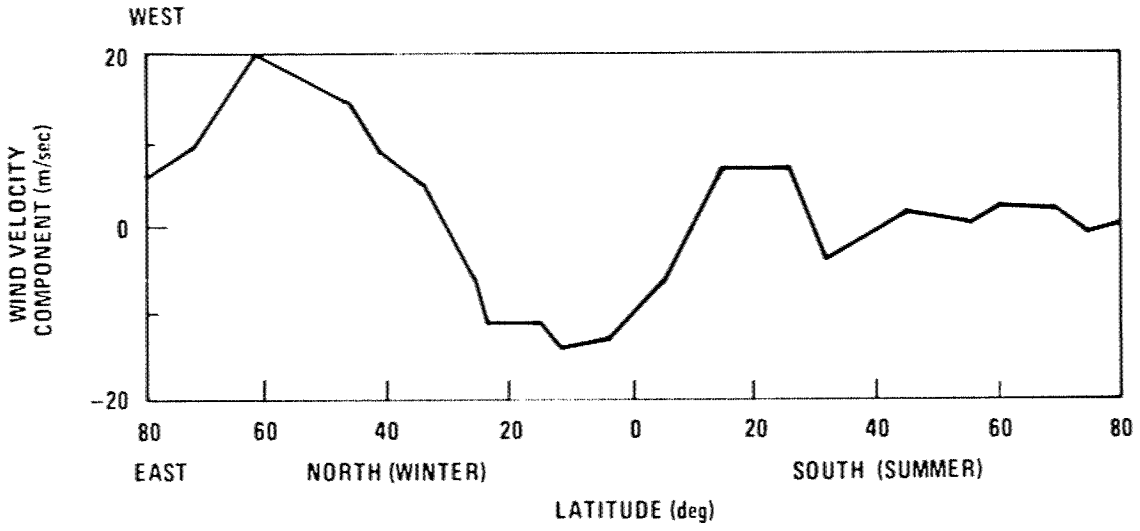

Figure 10. – Calculated Mean Zonal Component of Wind – Top of Surface Boundary Layer at Summer Solstice (ref. 87).

southern summer solstice. Their results for the southern summer solstice indicate that the meridional component of mean wind has a strong circulation across the equator. This meridional flow has a speed of 10 m/s with the southerly wind at high altitude and the northerly wind near the surface. Its effective region is between 25°N and 30°S latitudes. As a result of this flow pattern, the air mass is being transferred from the diminishing polar cap to the growing polar cap. The zonal component of the mean wind at near surface is illustrated in figure 10 where the easterly and westerly winds are plotted against latitudes. The mean flow in the summer hemisphere is expected to be stable and nearly undisturbed. For the winter hemisphere, however, the mean flow becomes unstable. Leovy and Mintz also found that the maximum instantaneous near-surface wind speed occurs at 20°S latitude and that the average speed of the extremely strong winds at 15 km altitude at 40°S is about 70 m/s.

The diurnal variation in wind velocity for a clear atmosphere has been explored by Goody (ref. 47). Goody pointed out that the diurnal variation of wind because of temperature changes is complicated by variations in tropopause height and eddy exchange coefficient and by the unknown behavior of the atmospheric tidal energy. The magnitude of this thermally-driven diurnal change of wind is estimated to be 2 m/s (ref. 88). However, the diurnal fluctuation in the vertical momentum exchange can cause a diurnal variation in wind velocity as large as the zonal wind itself, which has a magnitude of 40 m/s (ref. 88).

Large scale motions are known to have a significant effect on the atmospheric vertical temperature structure (e.g., refs. 89 through 92). Dynamic processes including baroclinic waves, vertical oscillations such as induced by topographic relief, and vertical oscillations at altitude were studied (ref. 93). These processes were shown to modify temperature structure predicted by radiative-convective model in such a way as to provide an explanation of the observed cold middle atmosphere (ref. 37) that was not predicted by the less complete models.

The vertical wind vector gradient in the Martian atmosphere has been investigated by Wood (ref. 20) who took the results of wind component at two levels provided by Leovy and Mintz and assumed a linear variation of wind with height. His analysis indicates that the vertical wind vector gradient is positive from the top of the surface boundary layer to 15 km altitude and negative for the altitude region above 15 km. The magnitude of the vertical wind vector gradient has been suggested to be 6 m/s-km for space vehicle design (ref. 94).

2.1.2 Upper Atmosphere

The only measurements that pertain directly to conditions in the upper atmosphere of Mars are the electron density profiles obtained from Mariner 4, 6, 7, and 9 and the ultraviolet airglow data obtained from Mariner 6, 7, and 9 and the USSR Mars 2 and 3. Therefore, engineering models for the upper atmosphere must rely on a variety of theoretical studies and inferences derived from limited data. The range in the models, however, has been narrowed considerably by spacecraft results.

2.1.2.1 Ionosphere

There has long been speculation that Mars has an ionosphere with a structure similar to that of Earth. A scientific discussion of the upper atmosphere of Mars, however, has only been possible since the successful experiment of Mariner 4. More information has been provided by Mariner 6, 7, and 9 experiments.

The formation of the Martian ionosphere and interpretation of electron number density data acquired from Mariner experiments are based on Earth analogy. As with the terrestrial atmosphere, the photoionization process on Mars is expected to form an ionosphere. The height and extent of the Martian ionosphere are complex functions of the season, solar activity, and time of day. In the uppermost regions of the atmosphere, the number density of the molecules is too low to produce an appreciable electron density. At lower altitudes, electron density is limited by attenuation of the ultraviolet radiation in the atmosphere and large electron recombination rates from increased density.

It has been concluded (ref. 20) that the electron number densities in the Martian ionosphere should not be large enough to affect radio communication to and from a lander on the surface. For spacecraft atmospheric entry, electron densities are not considered significant even behind the bow shock wave that forms by compression of the solar wind's magnetic field against the ionosphere (ref. 95).

A. Electron Density Data

Figure 11 shows the distributions of electron number-density in the Martian ionosphere from Mariner 4, 6, 7 and 9 (refs. 25, 29, and 97). The maximum electron densities are much lower than expected at altitudes of 120 km from Mariner 4 measurements, 135 km from Mariner 6 and 7 measurements, and 135 km from Mariner 9 data. This indicates a lower atmospheric temperature than anticipated.

The measured maximum electron density was 10^5 cm^{-3} from Mariner 4 when the solar activity was low and the solar zenith angle was large (67°). The Mariner 6 and 7 measure-

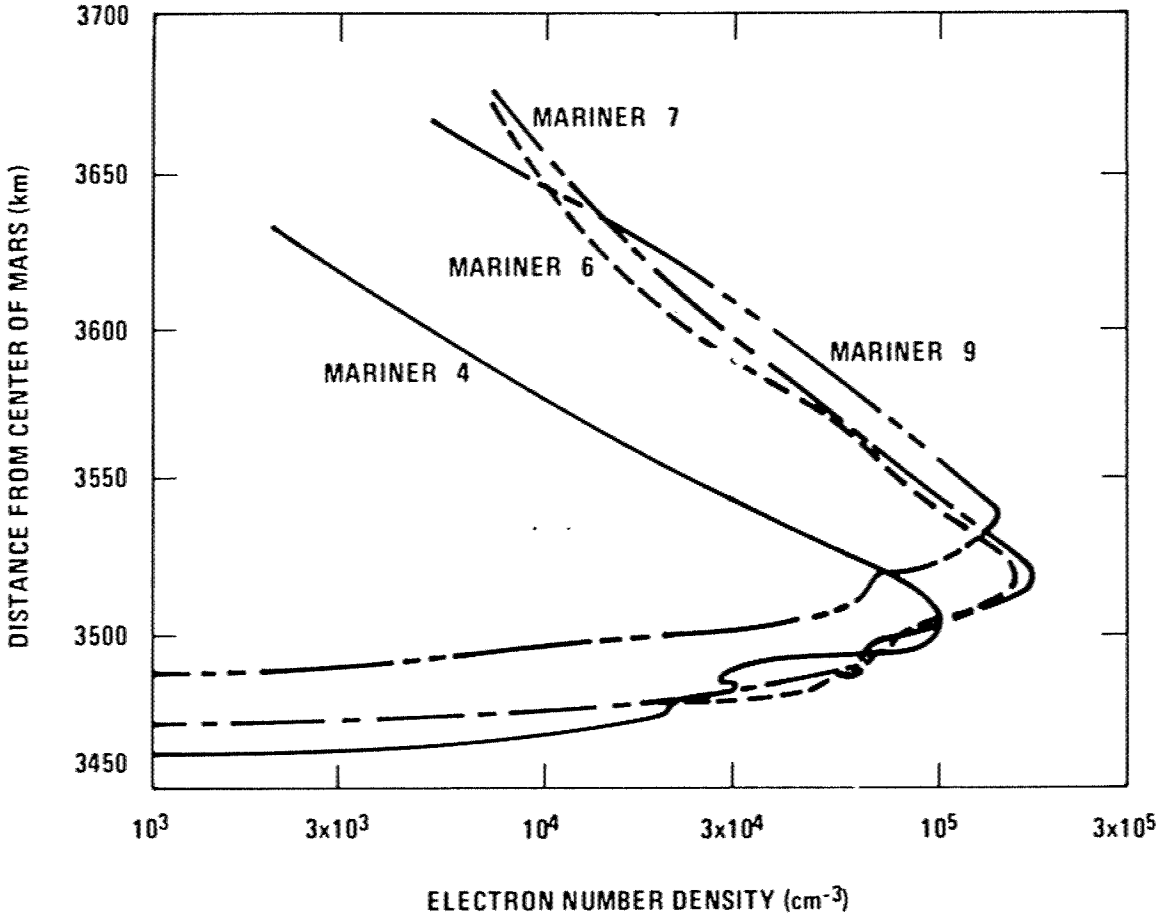

Figure 11.—Martian Ionization Profiles (refs. 25, 29, and 96).

ments gave a maximum electron density of 1.7×10^5 cm^{-3} when the solar activity was higher than in 1965. The Mariner 9 data shown are for revolution 12 at a solar zenith angle of approximately 55°. As the solar zenith angle decreased in subsequent revolutions, the electron maximum was observed to occur at lower altitudes and to be of greater density (ref. 29).

B. Major Constituents

The major ion in the Martian ionosphere is ionized molecular oxygen, O_2^+. This has been inferred from a combination of laboratory experiments and analysis of Mariner 6 and 7 data (ref. 97). O_2^+ is generated by the reaction of atomic oxygen ions, O^+ with carbon dioxide, CO_2. Figure 12 is a theoretical model of the Martian ionosphere that shows the relative densities of the principal constituents at different altitudes. For a concentration of one percent atomic oxygen, the ratio of O_2^+ to CO_2^+ is approximately 3 to 1 (ref. 98).

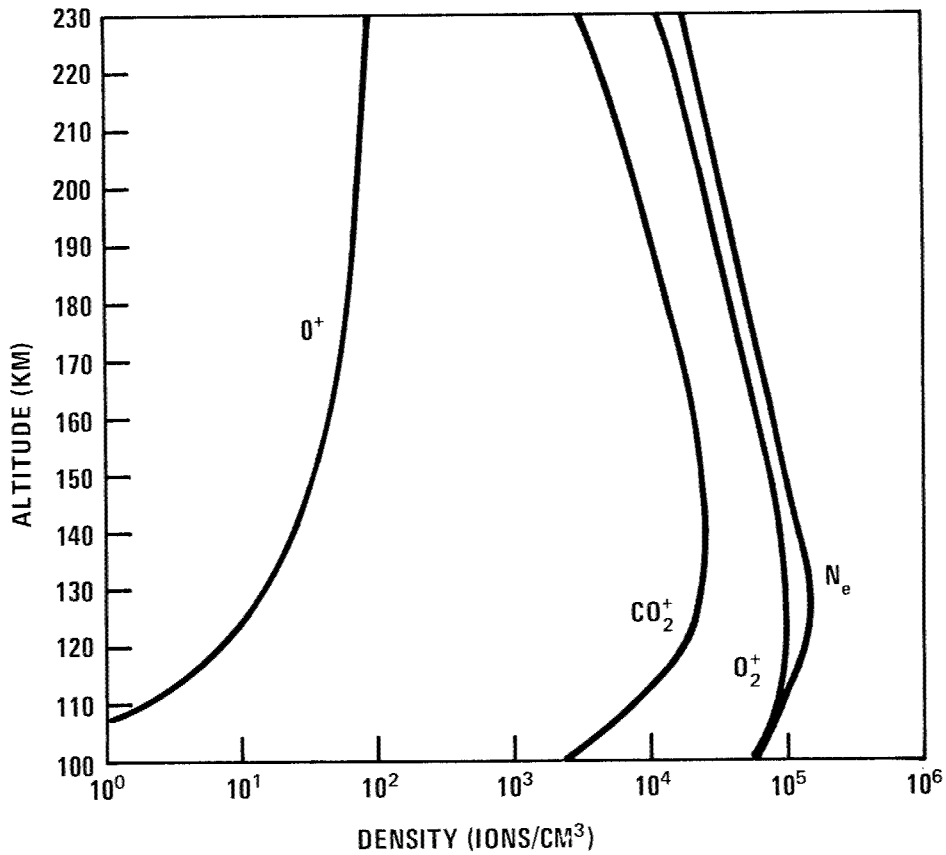

Figure 12.—Model of Martian Ionosphere Components (ref. 98).

C. Models

A preliminary one dimensional model for the interaction of the Martian ionosphere with the solar wind was presented by Cloutier et al. (ref. 99). Their model predicted a major depression of the ionospheric scale height that was associated with the pressure of lost shock solar plasma which was assumed to stream subsonically into the Martian upper ionosphere. The validity of the one dimensional model was not supported, however, by subsequent spacecraft results. More recent theoretical models have attempted to remove the one dimensional limitation.

Cloutier and Daniell (ref. 100) considered a model in which the magnetized solar wind acted as a dynamo over the day side of the planet. In this model the distribution of currents entering the ionosphere through the plasmapause was considered carefully. The location of the plasmapause was fixed by a requirement that the total ionospheric current must be of sufficient magnitude to cancel the shock-compressed interplanetary magnetic field. This requirement led to an estimated height of 320 to 425 km for the plasmapause.

An alternate model for the outer ionosphere was discussed by Bauer and Hartle (ref. 101). They noted evidence from the USSR spacecraft Mars 2 and 3 (ref. 102) for a weak intrinsic

magnetic field on Mars that could be of sufficient strength to balance the dynamic pressure of the solar wind at a height of about 1000 km. The distribution of plasma inside the magnetosphere would be controlled in large measure by the convective electric field induced by the solar wind except below 300 km where chemical processes are more efficient than electrodynamically-induced mass motion. A schematic illustration of the plasma flow pattern is given in figure 13 from reference 101. Bauer and Hartle estimated a plasmapause height of about 300 km.

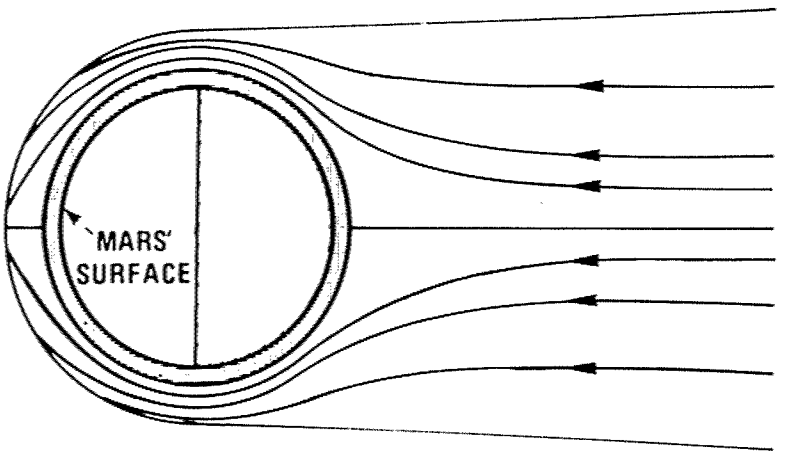

Figure 13. – Solar Wind-Induced Convective Flow Pattern for Mars (ref. 101).

From the foregoing models, therefore, one could conclude that because of interaction with the solar wind, the Martian ionosphere should terminate effectively between 300 and 450 km, the predicted range of altitudes for the plasmapause. One expects also that the solar wind should induce significant departures from photochemical equilibrium in the ionosphere at high latitudes and at large solar zenith angles; there are indications in the Mariner 9 data (refs. 78 and 103) that these departures may have been observed.

2.1.2.2 Neutral Atmosphere

Mariner 6, 7, and 9 carried ultraviolet spectrometers to measure radiations emitted by atomic hydrogen and atomic oxygen (refs. 98 and 104). The measured airglow spectrum is characteristic of an essentially pure CO_2 atmosphere. Almost all of the observed emissions were produced by the action of solar ultraviolet radiation on CO_2. Mars 2 and 3 also carried experiments to measure ultraviolet emissions of the atmosphere (ref. 105). The Mariner results showed the presence of carbon monoxide (CO), atomic carbon, atomic hydrogen, and atomic oxygen (ref. 98). The amount of atomic hydrogen at 135 km was calculated to be one part per million (ref. 106) and the amount of atomic oxygen at the same altitude is about one percent (ref. 107).

The density of atomic hydrogen at 200 km was calculated to be 3×10^4 atoms cm^{-3} (ref. 106) on the basis of Mariner 6 and 7 data. The temperature at the top of the Martian thermosphere (fig. 1) was determined to be 350 K from Mariner 6 and 7 data (ref. 108), 325 K from Mariner 9 data (ref. 109), and about 250 K from Mariner 4 data. The higher temperatures are associated with the higher values of extreme ultraviolet (EUV) radiation that occur in high-activity periods of the solar cycle.

Photodissociation of CO_2, electron-impact dissociation of CO_2, and dissociative recombination of CO_2^+ all produce atomic oxygen in the Martian upper atmosphere (ref. 98). Theoretically, it could be expected that atomic oxygen would be a dominant species; however, analysis of ionospheric profiles suggests that oxygen abundances at the ionospheric peak are less than ten percent, which is consistent with the one percent result of reference 107. The observed concentrations of O indicate that mixing processes must be exceedingly efficient in the upper Martian atmosphere. It may be estimated that the turbopause is located at an altitude as high as 150 km.

The major uncertainties in neutral densities of the upper atmosphere relate to the location of the turbopause and the abundance of light constituents O, N_2, CO, and He at the turbopause. Calculated densities for several known constituents are shown in figure 14, which is based on Mariner 6 and 7 observations (ref. 98). The turbopause in these models was set at 100 km. The amount of CO and O_2 in the model was based on the results of ground-based observations, that is, less than 0.1 percent for CO (ref. 49) and slightly more than 0.1 percent for O_2 (ref. 110). The expected low abundance of N_2 is discussed in section 2.1.1.2.

Theoretical attempts have been made to calculate temperatures for the upper Martian atmosphere with observed values for the flux of solar ultraviolet radiation and reasonable estimates for the rates of key chemical reactions. The resulting theoretical models tend to give temperature values that are higher than values of temperatures derived from analyses of ionospheric profiles and airglow data. For example, one theoretical thermal model (ref. 111) yielded an exospheric temperature of 487 K on the basis of Mariner 4 (solar flux) data (July 1965) as compared to 300 K that was derived from electron scale height by Stewart and Hogan (ref. 112). The difference was attributed to difficulties in estimating EUV heating efficiency and flux (ref. 111). An exospheric temperature of 500 K for July 1969 that was inferred from the electron scale height determined from Mariner 6 and 7 data (ref. 96) can be explained by greater EUV in 1969 than in 1965. It appears that the discrepancies may be removed by inclusion of eddy transport in the theoretical models although definitive results have not yet been reported.

2.1.3 Clouds

Clouds have been observed from Earth and have been verified by Mariner 6, 7, and 9 experiments, especially by television pictures. The cloud features are usually referred to as yellow, white, blue, and an ill-defined "blue haze".

The observed yellow clouds are generally considered to be associated with dust storms. Storms of local extent may become global, as observed by Mariner 9 in late 1971. The

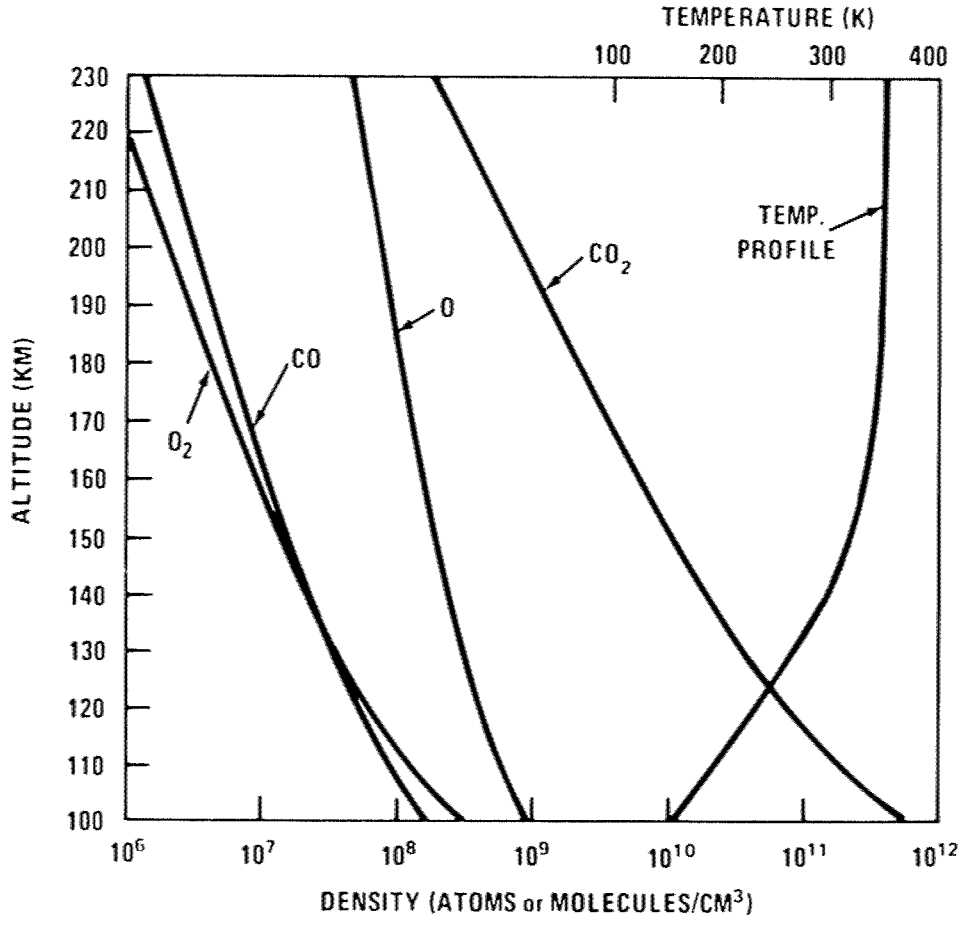

Figure 14.–Model of Martian Neutral Atmosphere Components (ref. 98).

global storm of 1971 extended from the surface to as high as 30 km. Particle size has been discussed in section 2.1.2.

Stationary clouds have been observed from the Earth and in Mariner 9 pictures over large calderas and other high topographical features (ref. 30). These white clouds begin to brighten in the early afternoon and continue to brighten until they disappear over the afternoon limb (ref. 113). These clouds have been correlated with features in the Tharsis, Olympus Mons, and Elysium regions. The timing of the clouds' appearance and their relationship to very high topography indicates that they may be formed by lifting of heated air from the surrounding lower terrain. These clouds may lie between 8 to 10 km above the surface and contain water ice (ref. 114). Water ice also has been detected in the spectrum of the north polar hood (ref. 115).

Another layer of white clouds has been identified in the polar region between about 5 and 30 km (ref. 116), which are generated in a wave configuration by flow over irregular topography. Topographic clouds persist north of 45° N during the northern late winter season. Two of the wave-cloud systems seen in Mariner 9 pictures near the periphery of the

north polar hood have been seen repeatedly from Earth and were detected by Mariner 6 and 7 (ref. 117). Mariner 6 and 7 measurements revealed reflection features near 4.3μ that are characteristic of solid CO_2 (ref. 118); however, from a combination of Mariner 9 imaging and IRIS data, it has been argued that most of the clouds observed between 45 and 60°N are composed mostly of water ice (ref. 116).

Brightness profiles and pictures from Mariner 9 indicate a cloud layer between 45 and 65 km. The layer is much bluer than the underlying dust (ref. 30). The clouds were observed near the 0.02 mb pressure level and had an estimated thickness of not more than 2 km. In the South polar region, it is suspected that water ice is the principal constituent and the clouds over the North polar hood appear to be composed of CO_2 ice, and possibly water ice.

A "blue haze" has been observed, but its location in the atmosphere and its properties are unknown. Surface details on Mars generally are clearly seen in any light of wavelengths greater than 4500 to 4550 Å, i.e., red or yellow light. The Martian "blue haze" is a diffuse, variable phenomenon that occasionally clears and allows surface features to be observed in blue light, sometimes described as "blue clearing". The haze itself, which is probably a high-altitude layer, is not blue but extinguishes solar blue light reflected from the Martian surface although transparent to longer wavelengths of light. When the effects of observational selection are removed, some workers believe that there is some correlation of blue clearing with favorable oppositions. The evidence is not compelling, however, because blue clearings have been observed also at unfavorable oppositions or several months from opposition and on small topographical scales of Mars down to the limit of telescopic resolution.

Some authorities discount the hypothesis that the "blue haze" is produced by scattering of light by condensed particles. They suggest that the "blue haze" and its occasional clearing may result from selective absorption of light by solid particles in the atmosphere. Others have suggested that interaction of solar wind protons with the CO_2 of the atmosphere causes the "blue haze" by producing molecular ions (CO_2^+ and CO^+) that have strong absorption bands in the required energies. These hypotheses are all speculative, however.

2.1.4 Gravity Field

If Mars is considered as an oblate spheroid, its gravitational potential function can readily be developed in a spherical harmonic series. Truncation after the first two terms gives the gravitational potential function as (ref. 119):

$$\phi(R, \theta) = \frac{GM}{R} [\, 1 - J_2 \, (R_E/R)^2 \, P_2^0 \,]$$

and the radial acceleration of gravity as

$$g = -\frac{\partial \phi}{\partial R} = \frac{GM}{R^2} [\, 1 - 3J_2 \, (R_E/R)^2 \, P_2^0 \,]$$

in which

$$P_2^0 = \frac{3}{2} \sin^2 \theta - \frac{1}{2}$$

θ	=	latitude
R_E	=	equatorial radius = 3394(±2) km
R	=	distance from center of Mars (km)
GM	=	42828.5 (±0.4) km^3/s^2
J_2	=	0.001965 (±0.000006)

The constant J_2 is a measure of the flattening, f = 0.00524 ± 0.00003. The foregoing values are incorporated from Mariner 9 results (ref. 120).

The centrifugal correction to the radial component of gravitational acceleration can be expressed as

$$F_c = \omega^2 \, R \cos^2 \theta$$

where ω is the Martian angular velocity, 0.7088218×10^{-4} radians/s.

2.2 Atmospheric Models

2.2.1 Calculation

The models presented in this monograph were generated by the computer program described in reference 121. The program was modified to include a molecular mass subroutine to handle the molecular mass variation with altitude, an extended temperature range for the calculation of the specific heat and the reduced collision integral which appears in the viscosity relationship, and thermochemical data that allow for the inclusion of atomic oxygen and atomic hydrogen as component gases.

The basic inputs to the computer program are the temperature profile, the surface pressure, the near-surface atmospheric composition and corresponding molecular mass, the planetary radius, the acceleration of gravity at the planet's surface, and the atmospheric density at the turbopause. The values for density, pressure, speed of sound, molecular mass, density scale height, number density, mean free path, viscosity, and pressure scale height as functions of altitude are calculated with the mathematical relationships given in reference 113; additional mathematical operations are required to determine the mean molecular mass values above the turbopause. All operations satisfy the hydrostatic equation and equation of state. Calculations account for the variation of gravitational acceleration with altitude throughout the atmosphere.

2.2.2 Choice of Model Parameters

Models were computed for the Martian atmosphere to account for uncertainties in atmospheric parameters. Table 2 shows the input parameters for the engineering models of the Mars atmosphere that have been developed. The lower portion of the atmosphere was based on temperature profiles determined from spacecraft measurements. In the upper atmosphere, temperature profiles were obtained from reference 122 which was based on the

thermal model of reference 108. The upper atmosphere temperature profiles were constrained at the lower end by density values at the turbopause and by the temperature profiles that were adopted for the lower atmosphere. The top of the upper atmosphere temperature profiles were constrained by exospheric temperatures based on spacecraft data. The temperature profiles used for the atmospheric models are shown in figure 15.

The adopted temperature profiles near their minima cross the solid-vapor phase boundary for CO_2, beyond which CO_2 cannot exist as a gas. This discrepancy in the data has not been resolved in the literature. The adopted profiles represent the data that is currently available.

2.2.2.1 Lower Atmosphere

Temperature profiles for the lower atmosphere have been established by spacecraft measurements (section 2.1.1.3). The mean temperature profile for the clear atmosphere is representative of Martian mid-latitudes at the mean surface level. The low temperature profile for the clear atmosphere is derived from polar region measurements given in reference 123. The high temperature profile for the clear atmosphere is that of Mariner 9, revolution 174 shown in figure 7. The temperature profile for the dusty atmosphere is taken from revolution 20 of Mariner 9 shown in figure 7; it is representative of high temperatures encountered during a global dust storm.

Uncertainties in atmospheric surface temperature and pressure are associated with topographic differences, latitude, longitude, time of day, and season. The selected profiles encompass extremes measured by Mariner 9. Computations were initiated at 10 km below the mean surface level to allow for topographic variation. The composition of the lower atmosphere was chosen as 98.8 percent CO_2, 1 percent N_2, 0.07 percent CO, and 0.13 percent O_2 on the basis of abundances given in table 1.

2.2.2.2 Upper Atmosphere

The lower boundary for the theoretical upper atmosphere is the turbopause. The turbopause is the altitude below which the atmospheric gases mix in constant proportions; above this altitude each constituent gas is taken to be in diffusive equilibrium, with number density decreasing with altitude at a rate that depends upon the molecular mass of the gas and the ambient atmospheric temperature. The density value at the turbopause was estimated on the basis of the composition taken for the lower atmosphere and an eddy diffusion coefficient of 1×10^8 cm^2/s. From the turbopause upward the atmospheric composition was modified by the addition of atomic oxygen O and atomic hydrogen H. The abundance of H was assumed to be the same for all models, whereas O was chosen as 1 percent to obtain a reasonable minimum density, 3 percent for the mean density, and 10 percent for a reasonable maximum density. The abundance of CO_2 was decreased according to the amount of O and H added. The models of the upper atmosphere are superposed on the lower atmosphere models at the turbopause.

TABLE 2.
COMPUTER INPUTS FOR MODELS OF MARS ATOMSPHERE (1974)

Parameters	MODEL I	II	III	IV
Planetary Radius (km)	3394	3394	3394	3394
Surface Gravity (cm/s^2)	371.8	371.8	371.8	371.8
Surface Pressure (mb)	4.95	4.95	4.95	4.95
Surface Temperature (K)	207.5	182.5	255.0	255.0
Composition (% by volume)				
Below Turbopause				
CO_2	98.8	98.8	98.8	98.8
N_2	1.0	1.0	1.0	1.0
CO	0.07	0.07	0.07	0.07
O_2	0.13	0.13	0.13	0.13
At Turbopause				
CO_2	95.8	97.8	88.8	95.8
N_2	1.0	1.0	1.0	1.0
CO	0.07	0.07	0.07	0.07
O_2	0.13	0.13	0.13	0.13
O	3.00	1.00	10.00	3.00
H	0.0001	0.0001	0.0001	0.0001
Molecular Mass (g/g-mole)				
Below Turbopause	43.82	43.82	43.82	43.82
At Turbopause	42.98	43.56	41.02	42.98
Density at Turbopause (g/cm^3)	1.46×10^{-12}	1.46×10^{-12}	1.46×10^{-12}	1.46×10^{-12}
Exospheric Temperature (K)	350	250	500	350

The upper constraint on the upper atmosphere models is the exospheric temperature which is a function of both diurnal heating and solar cycle heating. A value of 250K is used for a night-side atmosphere with minimum solar activity; 500K is used for maximum solar activity and day-side exospheric temperatures; and 350K is representative of mean conditions. The temperature profiles for the upper atmosphere for the different exospheric temperatures are shown in figure 15.

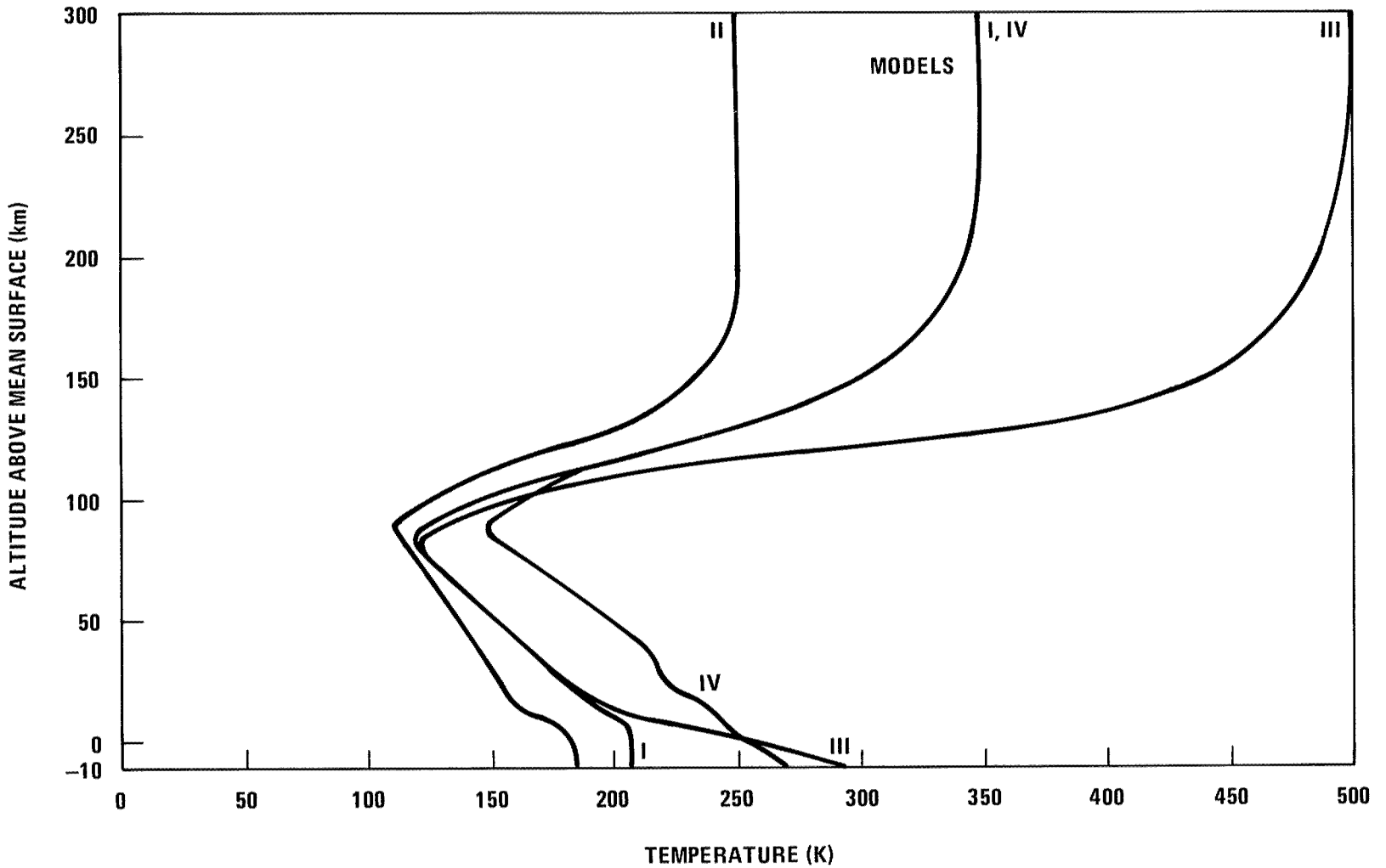

Figure 15. – Temperature Profile for Models of Mars' Atmosphere.

3. CRITERIA

The engineering models of the Mars atmosphere presented herein should be used for mission planning and design of space vehicles that are to orbit Mars, descend through the atmosphere, maneuver in the atmosphere, land on the planetary surface, or conduct scientific investigations during a planetary flyby mission. The models should be used for all facets of space vehicle design including

Structure
Deceleration system
Propulsion system
Flight control system
Guidance system
Heat shield and thermal control system
Communication systems
Electronics
Power supply
Mechanical devices
Scientific experiments (equipment and measurement ranges)

The models should be regarded as approximations that are based on the best available data and which encompass current uncertainties in the atmospheric parameters. The models are by necessity relatively general in nature; they are particularly useful for preliminary design and mission tradeoff studies. In later design stages, after specific missions, orbits, and landing sites are selected, the range of atmospheric parameters can be significantly reduced by specifying geographic location of landings, orbital parameters of satellites and subsatellites, season of the Martian year, Martian local time, and predicted level of solar activity for that time. If the foregoing information is known, it may be possible to select temperature profiles from Mariner 9 data that embody the effects of variation as to spatial coordinates, topography, season, time of day, and dust storms. The Mariner 9 temperature profiles from the Infrared Interferometer Spectroscopy (IRIS) spectra will be made available to the scientific community in 1975 through the National Space Science Data Center, NASA Goddard Space Flight Center (ref. 124).

3.1 Atmospheric Models

The engineering models of the Mars atmosphere are given in tables 3 through 6. Model I (table 3) should be considered as the nominal model. It is representative of clear atmospheric conditions at mid-latitudes in mid-spring or mid-autumn during periods of moderate solar activity. Models II through IV (tables 4 through 6) take into account possible extremes of molecular mass, solar activity, exospheric temperature and atmospheric clarity in appropriate combinations as shown in table 2. Model II (table 4) presents a cold temperature model with a low-density upper atmosphere. It is best applied in the polar regions, during winter, or for night-time analyses, all at periods of low solar activity. Model III (table 5) presents a high temperature model of the clear atmosphere with a high-density upper atmosphere. It is intended for application in equatorial regions, during summer, or for

afternoon analyses, during periods of high solar activity. Model IV (table 6) presents a temperature model of the atmosphere that can be considered as typical during global dust storms. Figures 4 and 5 give additional information on temperature variation with latitude, local time, and the presence of dust.

All models are based on a mean planetary radius of 3394 km which corresponds to 0 km altitude in the tables. However, to encompass possible extremes of local topography as well as variations in local radius, the tables have been extended downward to -10 km which corresponds to a planetary radius of 3084 km. Thus, if a model is applied to a low area such as the Hellas region, the tables would be entered at about -4 km or if a high region such as Olympus Mons is considered, the table is entered at about 28 km (fig. 2).

The four tables were terminated at altitudes where the density falls to 10^{-16} g/cm^3 because the hydrostatic equilibrium assumption upon which these models are based undoubtedly becomes invalid at greater altitudes.

3.2 Winds

Information on Martian winds was obtained from cloud observations, studies of dust storm characteristics, and models of atmospheric circulation and tidal pressure. The following near-surface wind speeds are recommended for space vehicle design purposes.

Wind Parameter	Surface Pressure	
	4 mb	8 mb
Mean Speed (1 m above surface)	50 m/s	35 m/s
Peak Speed	145 m/s	100 m/s
Vertical Wind Vector Gradient	6 m/s · km	6 m/s · km

3.3 Ionosphere

Observations by Mariner 4, 6, 7, and 9 spacecraft indicate peak electron density in the Martian ionosphere to be of the order of 10^5 cm^{-3}. This density should not be large enough to affect radio communication to and from a lander on the surface. For spacecraft atmospheric entry, electron densities should not be significant even behind the bow shock wave which forms through compression of the solar wind's magnetic field against the ionosphere. The electron density profiles given in figure 11 should be used in design configuration analyses.

3.4 Clouds

Distinct cloud layers, identified by color, have been verified by spacecraft television pictures. Cloud characteristics are summarized below.

Cloud Layer	Remarks	Altitude Above Mean Surface (km)	Composition
Yellow	Local and global dust storms	0-30	Surface dust; 10-300 μm
White-Low	High topographical features; late afternoon	8-10	Water ice
White-High	Wave clouds associated with irregular topography	5-30	Mostly water ice
Blue	Principally in polar regions	45-65	Water ice (south polar region); CO_2 ice and possibly water ice (north polar hood)
Blue Haze	Diffuse, variable phenomenon - usually visible; rapid changes in state - random from opacity to near transparency	Not uniform over entire atmosphere; probably high altitude	Not known; sources speculative

TABLE 3.*
1974 MARS ATMOSPHERE (MODEL I) (MEAN TEMPERATURE PROFILE).

Altitude (km)	Temperature (K)	Pressure (mb)	Density (g/cm^3)	Speed of Sound (m/s)	Molecular Weight	Density Scale Height (km)	Number Density (cm^{-3})	Mean Free Path (m)	Viscosity (kg/m · s) (E + 5)	Pressure Scale Height (km)
-10	207.5	1.28E+01	3.25E-05	230.	43.824	10.53	4.47E+17	3.23E-06	1.06	10.53
-8	207.5	1.06E+01	2.69E-05	230.	43.824	10.54	3.69E+17	3.91E-06	1.06	10.54
-6	207.5	8.75E+00	2.22E-05	230.	43.824	10.55	3.05E+17	4.73E-06	1.06	10.55
-4	207.5	7.24E+00	1.84E-05	230.	43.824	10.56	2.53E+17	5.71E-06	1.06	10.56
-2	207.5	5.99E+00	1.52E-05	230.	43.824	10.58	2.09E+17	6.90E-06	1.06	10.58
0	207.5	4.96E+00	1.26E-05	230.	43.824	10.59	1.73E+17	8.34E-06	1.06	10.59
2	207.5	4.11E+00	1.04E-05	230.	43.824	10.60	1.43E+17	1.01E-05	1.06	10.60
4	207.0	3.40E+00	8.66E-06	230.	43.824	10.72	1.19E+17	1.21E-05	1.06	10.59
6	206.0	2.81E+00	7.20E-06	229.	43.824	10.83	9.90E+16	1.46E-05	1.06	10.55
8	204.5	2.33E+00	6.00E-06	228.	43.824	10.90	8.24E+16	1.75E-05	1.04	10.48
10	202.0	1.92E+00	5.01E-06	227.	43.824	11.08	6.89E+16	2.10E-05	1.03	10.37
15	192.5	1.17E+00	3.21E-06	219.	43.824	10.74	4.41E+16	3.27E-05	.97	9.91
20	185.0	7.01E-01	2.00E-06	213.	43.824	10.21	2.75E+16	5.28E-05	.92	9.55
25	180.0	4.13E-01	1.21E-06	209.	43.824	9.83	1.66E+16	8.69E-05	.88	9.32
30	175.5	2.40E-01	7.21E-07	205.	43.824	9.61	9.91E+15	1.46E-04	.85	9.11
35	171.0	1.38E-01	4.25E-07	201.	43.824	9.40	5.84E+15	2.47E-04	.83	8.91
40	166.5	7.81E-02	2.47E-07	198.	43.824	9.05	3.40E+15	4.25E-04	.80	8.70
45	162.0	4.36E-02	1.42E-07	195.	43.824	8.91	1.95E+15	7.40E-04	.77	8.49
50	157.0	2.40E-02	8.16E-08	191.	43.824	8.71	1.11E+15	1.30E-03	.75	8.25
55	152.5	1.30E-02	4.49E-08	187.	43.824	8.44	6.17E+14	2.34E-03	.72	8.04
60	148.0	6.91E-03	2.46E-08	184.	43.824	8.21	3.38E+14	4.27E-03	.70	7.82
65	143.0	3.61E-03	1.33E-08	180.	43.824	8.00	1.83E+14	7.89E-03	.67	7.58
70	138.5	1.85E-03	7.54E-09	177.	43.824	7.73	9.67E+13	1.49E-02	.65	7.36
75	134.0	9.28E-04	3.65E-09	174.	43.824	7.50	5.02E+13	2.88E-02	.63	7.14
80	129.5	4.56E-04	1.86E-09	170.	43.824	7.27	2.55E+13	5.66E-02	.61	6.92
85	125.0	2.19E-04	9.22E-10	167.	43.824	7.04	1.27E+13	1.14E-01	.59	6.70
90	120.0	1.02E-04	4.49E-10	163.	43.824	6.82	6.17E+12	2.34E-01	.57	6.45
95	118.5	4.69E-05	2.09E-10	162.	43.824	6.49	2.87E+12	5.03E-01	.56	6.39
100	131.0	2.23E-05	8.99E-11	171.	43.824	6.24	1.24E+12	1.17E+00	.62	7.08
110	169.0	6.49E-06	2.02E-11	201.	43.824	7.62	2.78E+11	5.19E+00	.91	9.19
120	221.0	2.52E-06	6.31E-12	235.	43.824	9.42	8.26E+10	1.75E+01	1.11	12.09
130	254.0	1.17E-06	2.42E-12	252.	43.824	11.83	3.33E+10	4.33E+01	1.25	13.97
140	281.5	5.96E-07	1.09E-12	267.	42.864	13.61	1.53E+10	9.57E+01	1.39	15.92
150	301.5	3.26E-07	5.52E-13	277.	42.387	15.26	7.84E+09	1.87E+02	1.49	17.34
160	315.0	1.87E-07	2.98E-13	284.	41.767	16.67	4.29E+09	3.42E+02	1.55	18.49
170	324.5	1.10E-07	1.67E-13	291.	40.970	17.77	2.46E+09	5.96E+02	1.59	19.53
180	333.0	6.70E-08	9.67E-14	298.	39.365	18.63	1.46E+09	1.01E+03	1.63	20.66
190	338.0	4.18E-08	5.75E-14	305.	38.731	19.65	8.96E+08	1.64E+03	1.65	21.76
200	342.5	2.67E-08	3.50E-14	313.	37.251	20.44	5.65E+08	2.59E+03	1.67	23.06
210	345.5	1.76E-08	2.17E-14	321.	35.538	21.40	3.68E+08	3.99E+03	1.69	24.51
220	347.5	1.18E-08	1.38E-14	331.	33.525	22.42	2.47E+08	5.95E+03	1.70	25.20
230	348.5	8.18E-09	9.92E-15	342.	31.574	23.59	1.70E+08	8.63E+03	1.70	28.14
240	349.5	5.81E-09	6.89E-15	355.	29.471	24.85	1.20E+08	1.22E+04	1.71	30.40
250	350.0	4.24E-09	3.99E-15	368.	27.409	26.43	8.77E+07	1.67E+04	1.71	32.92
260	350.0	3.16E-09	2.77E-15	382.	25.473	28.31	6.55E+07	2.24E+04	1.71	35.61
270	350.0	2.41E-09	1.97E-15	396.	23.726	30.39	5.00E+07	2.94E+04	1.71	38.45
280	350.0	1.88E-09	1.43E-15	409.	22.206	32.75	3.89E+07	3.77E+04	1.71	41.30
290	350.0	1.49E-09	1.07E-15	421.	20.925	35.36	3.08E+07	4.77E+04	1.71	44.07
300	350.0	1.19E-09	8.14E-16	432.	19.872	38.14	2.47E+07	5.95E+04	1.71	46.66
310	350.0	9.67E-10	6.32E-16	442.	19.024	40.97	2.00E+07	7.33E+04	1.71	49.00
320	350.0	7.92E-10	4.99E-16	450.	18.351	43.76	1.64E+07	8.95E+04	1.71	51.07
330	350.0	6.53E-10	4.00E-16	456.	17.823	46.40	1.35E+07	1.09E+05	1.71	52.87
340	350.0	5.42E-10	3.24E-16	462.	17.412	48.84	1.12E+07	1.31E+05	1.71	54.41
350	350.0	4.52E-10	2.66E-16	466.	17.093	51.01	9.35E+06	1.57E+05	1.71	55.72
360	350.0	3.79E-10	2.19E-16	469.	16.845	52.92	7.84E+06	1.87E+05	1.71	56.84
370	350.0	3.18E-10	1.82E-16	472.	16.655	54.57	6.58E+06	2.23E+05	1.71	57.80
380	350.0	2.68E-10	1.52E-16	474.	16.506	55.99	5.54E+06	2.65E+05	1.71	58.63
390	350.0	2.26E-10	1.27E-16	476.	16.389	57.20	4.68E+06	3.14E+05	1.71	59.36
400	350.0	1.91E-10	1.07E-16	477.	16.295	58.23	3.96E+06	3.71E+05	1.71	60.02
410	350.0	1.62E-10	9.03E-17	478.	16.222	59.12	3.35E+06	4.38E+05	1.71	60.61

*A one-or two-digit number (preceded by E and a plus or minus sign) following an entry indicates the power of ten by which that entry should be multiplied.

TABLE 4.*
1974 MARS ATMOSPHERE (MODEL II) (LOW TEMPERATURE PROFILE).

Altitude (km)	Temperature (K)	Pressure (mb)	Density (g/cm³)	Speed of Sound (m/s)	Molecular Weight	Density Scale Height (km)	Number Density (cm⁻³)	Mean Free Path (m)	Viscosity (kg/m-s) (E-5)	Pressure Scale Height (km)
-10	[illegible]	[illegible]	[illegible]	215.	[illegible]	9.53	[illegible]	[illegible]	.32	9.41
-8	188.0	[illegible]	[illegible]	214.	[illegible]	9.62	[illegible]	[illegible]	[illegible]	[illegible]
-6	186.?	[illegible]	[illegible]	212.	[illegible]	9.66	[illegible]	[illegible]	[illegible]	9.32
-4	184.0	7.600E+00	[illegible]	212.	[illegible]	9.49	[illegible]	[illegible]	[illegible]	[illegible]
-2	183.0	6.336E+00	[illegible]	211.	[illegible]	9.57	[illegible]	[illegible]	[illegible]	9.33
0	[illegible]	4.966E+00	[illegible]	[illegible]	[illegible]	9.43	[illegible]	[illegible]	[illegible]	9.31
2	182.0	4.000E+00	1.161E-05	210.	[illegible]	9.42	[illegible]	[illegible]	.30	9.30
4	181.0	3.735E+00	[illegible]	209.	[illegible]	9.5?	[illegible]	[illegible]	.59	[illegible]
6	179.0	[illegible]	[illegible]	[illegible]	[illegible]	9.66	[illegible]	[illegible]	[illegible]	9.17
8	177.0	[illegible]	[illegible]	206.	[illegible]	9.56	[illegible]	[illegible]	[illegible]	9.07
10	173.0	1.672E+00	[illegible]	203.	[illegible]	9.50	[illegible]	[illegible]	[illegible]	8.88
15	167.0	9.335E-01	[illegible]	198.	[illegible]	9.35	[illegible]	[illegible]	.75	8.79
20	[illegible]	[illegible]	1.72?E-06	191.	[illegible]	8.41	2.340E+16	[illegible]	[illegible]	8.28
25	154.0	2.73?E-01	[illegible]	189.	[illegible]	8.09	[illegible]	[illegible]	.77	7.99
30	151.0	1.455E-01	[illegible]	185.	[illegible]	8.16	6.97?E+15	[illegible]	.71	7.84
35	148.0	[illegible]	[illegible]	184.	[illegible]	7.91	[illegible]	[illegible]	[illegible]	7.71
40	145.0	3.365E-02	[illegible]	182.	[illegible]	7.88	[illegible]	7.27?E-04	.68	7.57
45	[illegible]	[illegible]	[illegible]	180.	[illegible]	7.67	[illegible]	[illegible]	.67	7.47
50	139.0	[illegible]	[illegible]	177.	[illegible]	7.58	[illegible]	2.67?E-03	.65	7.30
55	[illegible]	[illegible]	[illegible]	176.	[illegible]	7.39	[illegible]	[illegible]	[illegible]	7.19
60	[illegible]	[illegible]	[illegible]	173.	[illegible]	7.30	[illegible]	[illegible]	.63	7.03
65	[illegible]	[illegible]	[illegible]	171.	[illegible]	7.10	[illegible]	[illegible]	.61	[illegible]
70	[illegible]	[illegible]	[illegible]	169.	[illegible]	7.00	[illegible]	[illegible]	[illegible]	[illegible]
75	[illegible]	[illegible]	[illegible]	[illegible]	[illegible]	[illegible]	[illegible]	[illegible]	[illegible]	[illegible]
80	[illegible]	[illegible]	[illegible]	[illegible]	[illegible]	[illegible]	[illegible]	[illegible]	.57	[illegible]
85	[illegible]	[illegible]	[illegible]	[illegible]	[illegible]	[illegible]	[illegible]	[illegible]	[illegible]	[illegible]
90	[illegible]	[illegible]	[illegible]	160.	[illegible]	[illegible]	[illegible]	[illegible]	.55	5.21
95	[illegible]	[illegible]	[illegible]	157.	[illegible]	[illegible]	[illegible]	[illegible]	.53	[illegible]
100	[illegible]	[illegible]	[illegible]	[illegible]	[illegible]	[illegible]	[illegible]	[illegible]	[illegible]	[illegible]
110	[illegible]	[illegible]	[illegible]	[illegible]	[illegible]	[illegible]	[illegible]	[illegible]	[illegible]	[illegible]
120	[illegible]	[illegible]	[illegible]	[illegible]	[illegible]	[illegible]	[illegible]	[illegible]	[illegible]	[illegible]
130	[illegible]	[illegible]	[illegible]	[illegible]	[illegible]	5.37	[illegible]	[illegible]	[illegible]	[illegible]
140	[illegible]	[illegible]	[illegible]	[illegible]	[illegible]	[illegible]	[illegible]	[illegible]	[illegible]	[illegible]
150	[illegible]	[illegible]	[illegible]	[illegible]	[illegible]	12.47	[illegible]	[illegible]	[illegible]	[illegible]
160	[illegible]	[illegible]	[illegible]	[illegible]	[illegible]	[illegible]	[illegible]	[illegible]	1.21	[illegible]
170	[illegible]	[illegible]	[illegible]	[illegible]	[illegible]	14.11	[illegible]	[illegible]	[illegible]	[illegible]
180	250.0	3.488E-09	[illegible]	[illegible]	[illegible]	14.90	[illegible]	[illegible]	[illegible]	[illegible]
190	[illegible]	[illegible]	[illegible]	[illegible]	[illegible]	[illegible]	[illegible]	[illegible]	[illegible]	[illegible]
200	[illegible]	[illegible]	[illegible]	[illegible]	[illegible]	16.47	[illegible]	[illegible]	[illegible]	[illegible]
210	[illegible]	[illegible]	[illegible]	[illegible]	[illegible]	[illegible]	[illegible]	[illegible]	[illegible]	[illegible]
220	250.3	4.333E-10	5.646E-16	[illegible]	[illegible]	18.94	[illegible]	[illegible]	[illegible]	[illegible]
230	[illegible]	[illegible]	[illegible]	[illegible]	[illegible]	[illegible]	[illegible]	[illegible]	[illegible]	[illegible]
240	[illegible]	[illegible]	[illegible]	[illegible]	[illegible]	22.93	[illegible]	[illegible]	[illegible]	23.72
250	[illegible]	[illegible]	[illegible]	[illegible]	[illegible]	[illegible]	[illegible]	[illegible]	[illegible]	[illegible]
260	[illegible]	[illegible]	[illegible]	[illegible]	[illegible]	28.26	[illegible]	[illegible]	[illegible]	33.63

*Where a two-digit number preceded by E and a plus or minus sign following an entry, indicates the power of ten by which that entry should be multiplied.

TABLE 5.*
1974 MARS ATMOSPHERE (MODEL III) (HIGH TEMPERATURE PROFILE).

Altitude (km)	Temperature (K)	Pressure (mb)	Density (g/cm^3)	Speed of Sound (m/s)	Molecular Weight	Density Scale Height (km)	Number Density (cm^{-3})	Mean Free Path (m)	Viscosity (kg/m · s) (E + 5)	Pressure Scale Height (km)
-10	295.0	1.02E+01	1.81E-05	269.	43.824	10.48	2.49E+17	5.76E-06	1.45	14.96
-8	287.5	8.87E+00	1.63E-05	266.	43.824	16.33	2.23E+17	6.46E-06	1.42	14.60
-6	279.3	7.72E+00	1.46E-05	263.	43.824	18.10	2.01E+17	7.21E-06	1.38	14.19
-4	271.0	6.69E+00	1.33E-05	259.	43.824	17.32	1.79E+17	8.08E-06	1.34	13.80
-2	260.5	5.77E+00	1.17E-05	255.	43.824	18.13	1.60E+17	9.00E-06	1.29	13.28
0	255.0	4.96E+00	1.02E-05	252.	43.824	15.14	1.41E+17	1.03E-05	1.26	13.01
2	245.5	4.24E+00	9.10E-06	248.	43.824	16.56	1.25E+17	1.16E-05	1.22	12.54
4	237.5	3.60E+00	8.00E-06	244.	43.824	15.27	1.11E+17	1.31E-05	1.18	12.15
6	229.0	3.05E+00	7.02E-06	240.	43.824	14.99	9.64E+16	1.50E-05	1.15	11.73
8	220.5	2.56E+00	6.12E-06	236.	43.824	14.45	8.42E+16	1.72E-05	1.11	11.30
10	213.5	2.14E+00	5.28E-06	233.	43.824	13.36	7.26E+16	1.99E-05	1.08	10.98
15	198.5	1.33E+00	3.54E-06	225.	43.824	12.09	4.87E+16	2.97E-05	1.01	10.22
20	188.0	8.07E-01	2.26E-06	215.	43.824	10.82	3.11E+16	4.64E-05	.94	9.71
25	181.0	4.77E-01	1.39E-06	209.	43.824	9.88	1.91E+16	7.56E-05	.89	9.37
30	175.5	2.78E-01	8.35E-07	205.	43.824	9.61	1.15E+16	1.26E-04	.85	9.11
35	171.0	1.60E-01	4.92E-07	201.	43.824	9.40	6.76E+15	2.14E-04	.83	8.91
40	166.5	9.04E-02	2.88E-07	198.	43.824	9.15	3.93E+15	3.67E-04	.80	8.70
45	162.0	5.05E-02	1.64E-07	195.	43.824	8.91	2.29E+15	6.39E-04	.77	8.49
50	157.0	2.78E-02	9.33E-08	191.	43.824	8.71	1.23E+15	1.13E-03	.75	8.25
55	152.5	1.50E-02	5.20E-08	187.	43.824	8.44	7.14E+14	2.02E-03	.72	8.04
60	148.0	8.00E-03	2.85E-08	184.	43.824	8.21	3.92E+14	3.69E-03	.70	7.82
65	143.0	4.18E-03	1.54E-08	180.	43.824	8.00	2.12E+14	6.82E-03	.67	7.58
70	138.5	2.14E-03	8.15E-09	177.	43.824	7.72	1.12E+14	1.29E-02	.65	7.36
75	134.0	1.07E-03	4.23E-09	174.	43.824	7.50	5.81E+13	2.49E-02	.63	7.14
80	129.5	5.28E-04	2.15E-09	170.	43.824	7.27	2.95E+13	4.89E-02	.61	6.92
85	125.0	2.53E-04	1.07E-09	167.	43.824	7.04	1.47E+13	9.94E-02	.59	6.70
90	120.0	1.18E-04	5.20E-10	163.	43.824	6.82	7.15E+12	2.02E-01	.57	6.45
95	123.0	5.51E-05	2.36E-10	165.	43.824	6.43	3.28E+12	4.45E-01	.58	6.63
100	140.5	2.73E-05	1.02E-10	179.	43.824	6.39	1.41E+12	1.03E+00	.66	7.65
110	196.5	9.04E-06	2.43E-11	223.	43.824	8.20	3.33E+11	4.33E+00	1.00	10.59
120	290.0	4.21E-06	7.66E-12	287.	43.824	10.50	1.05E+11	1.37E+01	1.43	13.85
130	374.0	2.43E-06	3.42E-12	299.	43.824	14.08	4.70E+10	3.07E+01	1.82	20.57
140	417.0	1.53E-06	1.94E-12	314.	43.824	18.65	2.66E+10	5.42E+01	2.12	23.67
150	442.0	1.02E-06	1.13E-12	337.	40.739	22.12	1.67E+10	9.12E+01	2.12	26.45
160	458.0	7.06E-07	7.41E-13	346.	39.955	24.31	1.12E+10	1.38E+02	2.17	23.11
170	468.5	4.99E-07	5.00E-13	354.	39.052	25.99	7.72E+09	1.97E+02	2.21	29.58
180	476.5	3.59E-07	3.44E-13	361.	38.325	27.26	5.45E+09	2.79E+02	2.24	31.37
190	482.0	2.62E-07	2.41E-13	369.	36.875	28.51	3.94E+09	3.87E+02	2.26	32.59
200	486.0	1.94E-07	1.71E-13	377.	35.637	29.66	2.93E+09	5.28E+02	2.29	34.25
210	489.0	1.46E-07	1.23E-13	385.	34.238	30.79	2.16E+09	7.04E+02	2.29	36.01
220	491.5	1.11E-07	8.94E-14	395.	32.789	31.95	1.64E+09	9.28E+02	2.30	38.01
230	493.0	8.63E-08	6.59E-14	405.	31.289	33.32	1.27E+09	1.20E+03	2.31	40.17
240	496.0	6.78E-08	4.89E-14	416.	29.775	34.41	9.90E+08	1.54E+03	2.32	42.71
250	497.5	5.40E-08	3.69E-14	427.	28.282	36.31	7.86E+08	1.94E+03	2.33	45.35
260	499.0	4.36E-08	2.82E-14	439.	26.840	38.06	6.33E+08	2.41E+03	2.33	48.19
270	500.0	3.56E-08	2.18E-14	451.	25.477	40.15	5.15E+08	2.95E+03	2.34	51.15
280	500.0	2.95E-08	1.72E-14	463.	24.213	42.60	4.27E+08	3.57E+03	2.34	54.11
290	500.0	2.46E-08	1.37E-14	474.	23.061	44.95	3.57E+08	4.27E+03	2.34	57.12
300	500.0	2.08E-08	1.10E-14	485.	22.028	47.50	3.01E+08	5.07E+03	2.34	60.13
310	500.0	1.76E-08	8.96E-15	496.	21.116	50.23	2.55E+08	5.96E+03	2.34	63.27
320	500.0	1.51E-08	7.39E-15	505.	20.321	53.11	2.19E+08	6.96E+03	2.34	65.89
330	500.0	1.30E-08	6.15E-15	514.	19.635	56.07	1.88E+08	8.08E+03	2.34	69.56
340	500.0	1.13E-08	5.17E-15	522.	19.048	59.08	1.64E+08	9.32E+03	2.34	71.85
350	500.0	9.83E-09	4.38E-15	529.	18.550	62.06	1.42E+08	1.07E+04	2.34	73.35
360	500.0	8.59E-09	3.75E-15	535.	18.130	64.98	1.24E+08	1.22E+04	2.34	75.45
370	500.0	7.54E-09	3.22E-15	540.	17.778	67.79	1.09E+08	1.40E+04	2.34	77.36
380	500.0	6.63E-09	2.79E-15	545.	17.483	70.44	9.61E+07	1.59E+04	2.34	79.08
390	500.0	5.85E-09	2.43E-15	549.	17.237	72.93	8.48E+07	1.80E+04	2.34	80.63
400	500.0	5.18E-09	2.12E-15	552.	17.032	75.22	7.50E+07	2.02E+04	2.34	82.03
410	500.0	4.59E-09	1.86E-15	555.	16.862	77.33	6.64E+07	2.28E+04	2.34	83.30
420	500.0	4.07E-09	1.64E-15	557.	16.720	79.25	5.93E+07	2.56E+04	2.34	84.45
430	500.0	3.62E-09	1.45E-15	559.	16.603	80.99	5.24E+07	2.91E+04	2.34	85.49
440	500.0	3.22E-09	1.28E-15	561.	16.505	82.57	4.67E+07	3.27E+04	2.34	86.45
450	500.0	2.87E-09	1.13E-15	562.	16.424	83.99	4.15E+07	3.68E+04	2.34	87.33
460	500.0	2.56E-09	1.01E-15	563.	16.356	85.28	3.71E+07	4.11E+04	2.34	88.15
470	500.0	2.29E-09	8.97E-16	564.	16.299	86.46	3.31E+07	4.60E+04	2.34	88.91
480	500.0	2.05E-09	8.00E-16	565.	16.252	87.53	2.96E+07	5.14E+04	2.34	89.63
490	500.0	1.83E-09	7.14E-16	566.	16.212	88.51	2.65E+07	5.75E+04	2.34	90.32
500	500.0	1.64E-09	6.38E-16	566.	16.179	89.42	2.37E+07	6.42E+04	2.34	90.97
510	500.0	1.47E-09	5.71E-16	567.	16.151	90.26	2.13E+07	7.16E+04	2.34	91.60
520	500.0	1.32E-09	5.11E-16	567.	16.127	91.05	1.91E+07	7.98E+04	2.34	92.20
530	500.0	1.18E-09	4.58E-16	567.	16.107	91.79	1.71E+07	8.89E+04	2.34	92.79
540	500.0	1.06E-09	4.11E-16	568.	16.089	92.49	1.54E+07	9.90E+04	2.34	93.37
550	500.0	9.53E-10	3.69E-16	568.	16.074	93.16	1.38E+07	1.10E+05	2.34	93.93
560	500.0	8.58E-10	3.32E-16	568.	16.061	93.81	1.24E+07	1.23E+05	2.34	94.48
570	500.0	7.72E-10	2.98E-16	569.	16.050	94.43	1.12E+07	1.36E+05	2.34	95.03
580	500.0	6.96E-10	2.68E-16	569.	16.040	95.03	1.01E+07	1.51E+05	2.34	95.57
590	500.0	6.27E-10	2.42E-16	569.	16.031	95.61	9.03E+06	1.68E+05	2.34	96.11
600	500.0	5.65E-10	2.18E-16	569.	16.023	96.18	8.13E+06	1.86E+05	2.34	96.64
610	500.0	5.09E-10	1.96E-16	569.	16.015	96.74	7.33E+06	2.06E+05	2.34	97.17
620	500.0	4.60E-10	1.77E-16	569.	16.008	97.29	6.66E+06	2.28E+05	2.34	97.71
630	500.0	4.15E-10	1.60E-16	569.	16.001	97.83	6.01E+06	2.53E+05	2.34	98.23
640	500.0	3.75E-10	1.44E-16	569.	15.995	98.37	5.43E+06	2.80E+05	2.34	98.75
650	500.0	3.39E-10	1.30E-16	570.	15.989	98.90	4.91E+06	3.10E+05	2.34	99.28
660	500.0	3.07E-10	1.18E-16	570.	15.982	99.43	4.44E+06	3.43E+05	2.34	99.81
670	500.0	2.77E-10	1.07E-16	570.	15.976	99.96	4.02E+06	3.79E+05	2.34	100.35
680	500.0	2.51E-10	9.65E-17	570.	15.970	100.48	3.64E+06	4.19E+05	2.34	100.88

*A one-or two-digit number (preceded by E and a plus or minus sign) following an entry indicates the power of ten by which that entry should be multiplied.

TABLE 6.*
1974 MARS ATMOSPHERE (MODEL IV)
(TYPICAL DUSTY ATMOSPHERE TEMPERATURE PROFILE).

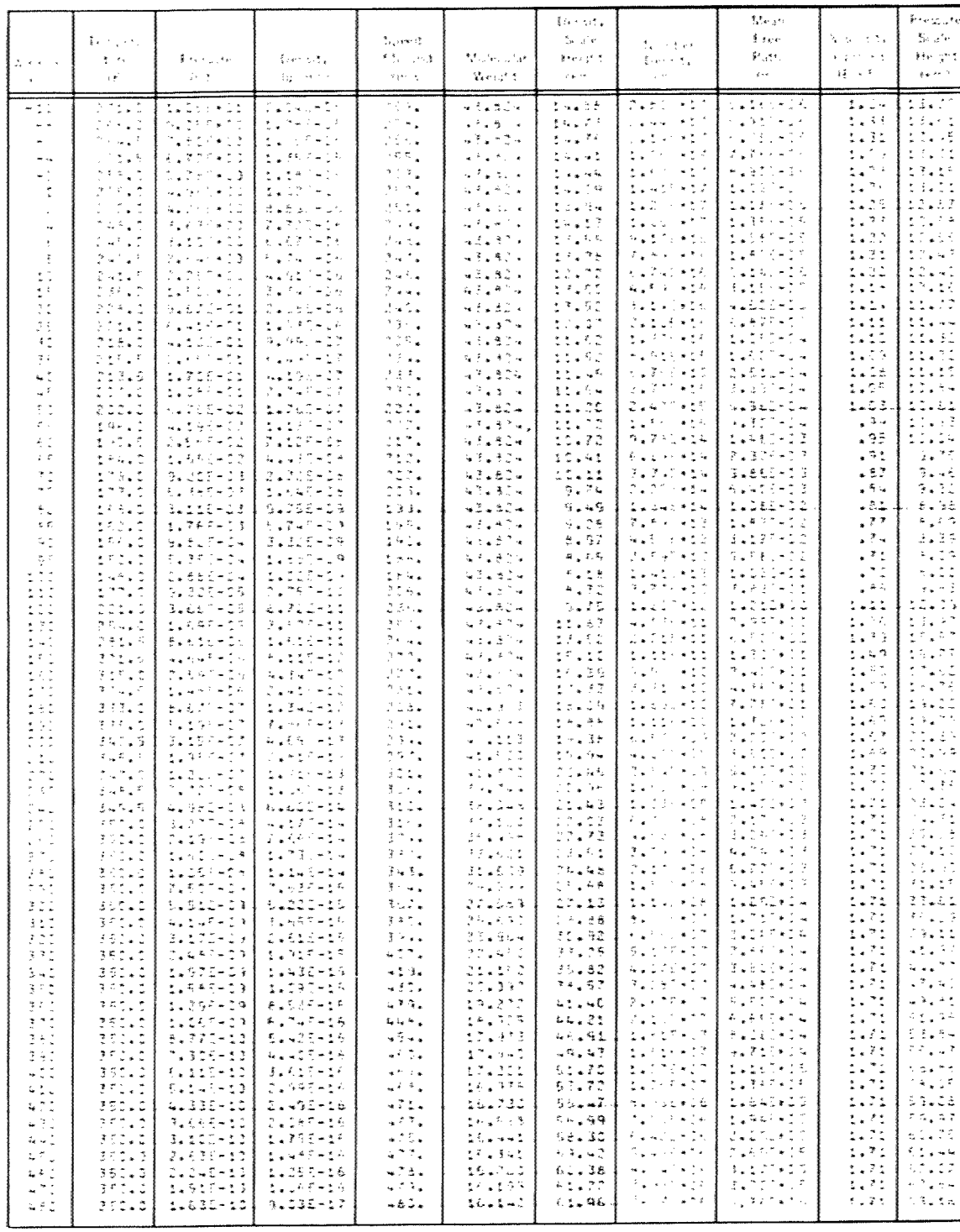

REFERENCES

1. Ingersoll, A. P.; and Leovy, C. B.: The Atmospheres of Mars and Venus. Annual Reviews of Astronomy and Astrophysics, Vol. 9, 1971, pp. 147-182.

2. Anon.: Models of Mars Atmosphere (1967). NASA Space Vehicle Design Criteria (Environment). NASA SP-8010, May 1968.

3. Levin, G. M.; Evans, D. E.; and Stevens, V.: NASA Engineering Models of the Mars Atmosphere for Entry Vehicle Design. NASA Technical Note D-2525, 1964.

4. Vachon, D. N.: Design Environments for Missions to Mars. General Electric Company Space Physics Component Technical Memo. No. 8126-8, 1966.

5. Evans, D. E.; Pitts, D. E.; and Kraus, G. L.: Venus and Mars Nominal Natural Environment for Advanced Manned Planetary Mission Programs. NASA SP-3016, 1967.

6. Anon.: Mars Engineering Model. NASA Langley Research Center, Viking Project Office M75-125-1, December 1970.

7. Anon.: Models of Venus Atmosphere (1972). NASA Space Vehicle Design Criteria (Environment). NASA SP-8011, revised September 1972.

8. Weaver, K. F.: Journey to Mars. National Geographic, Vol. 143, No. 2, February 1973, pp. 231-263.

9. Anon.: Mariner Mars 1971 Project Final Report; Vol. IV – Science Results. Jet Propulsion Laboratory, Technical Report 32-1550, Vol. IV, July 15, 1973.

10. Kaplan, L. D.; Munch, G.; and Sprinrad, H.: An Analysis of the Spectrum of Mars. Astrophysical Journal, Vol. 139, 1964, pp.1-15.

11. Gray, L. D.: Transmission of the Atmosphere of Mars in the Region of 2μ. ICARUS, Vol. 5, 1966, pp. 390-398.

12. Belton, M. J. S.; and Hunten, D. M.: The Abundance and Temperature of CO_2 in the Martian Atmosphere. Astrophysical Journal, Vol. 145, 1966, pp. 454-467.

13. Corlin, W. R.: Space Problems and Planetary Exploration. D. Van Nostrand Company, Inc., New York, 1965.

14. Kaula, W. M.: An Introduction to Planetary Physics. John Wiley & Sons, Inc., New York, 1968.

15. Grandjean, J.; and Goody, R. M.: The Concentration of Carbon Dioxide in the Atmosphere of Mars. Astrophysical Journal, Vol. 121, 1955, pp. 548-552.

16. Goody, R. M.: The Atmosphere of Mars. Weather, Vol. 12, 1957, pp. 3-15.

17. Musman, S.: An Upper Limit to a Rayleigh Scattering Atmosphere on Mars. Planetary Space Sciences, Vol. 12, 1964, pp. 799, 800.

18. Evans, D.: Ultraviolet Reflectivity of Mars. Science, Vol. 149, 1965, pp. 969-972.

19. de Vaucouleurs, G.: Physics of the Planet Mars. Faber & Faber, London, 1954.

20. Wood, G. P.: Mars Environment. In Mars Engineering Model for Viking Project, NASA Langley Research Center M75-125-1, 1970.

21. Fjeldbo, G.; Fjeldbo, W. C.; and Eshleman, V. R.: Models for the Atmosphere of Mars Based on the Mariner IV Occultation Experiment. J. G. R., Vol. 71, No. 9, 1966, pp. 2307-2316.

22. Fjeldbo, G.: Fjeldbo, W. C.; and Eshleman, V. R.: Atmosphere of Mars: Mariner IV Models Compared. Science, Vol. 153, 1966, pp. 1518-1523.

23. Kliore, A.; Fjeldbo, G.; and Seidel, B. L.: Mariner 6 and 7: Radio Occultation Measurements of the Atmosphere of Mars. Science, Vol. 166, 1969, pp. 1393-1397.

24. Rasool, S. I.; Hogan, J. S.; and Stewart, R. W.: Temperature Distributions in the Lower Atmosphere of Mars from Mariner 6 and 7 Radio Occultation Data. Journal of Atmospheric Sciences, Vol. 27, 1970, pp. 841-843.

25. Fjeldbo, G.; and Eshleman, V. R.: The Atmosphere of Mars Analyzed by Integral Inversion of the Mariner IV Occultation Data. Planetary Space Science, Vol. 16, No. 8, 1968, pp. 1035-1059.

26. Kliore, A. J.; Fjeldbo, G.; and Seidel, B. L.: Summary of Mariner 6 and 7 Radio Occultation Results on the Atmosphere of Mars. Paper No. M25 presented at the XIII Plenary Meeting of COSPAR, Leningrad, 1970.

27. Belton, M. J. S.; and Hunten, D. M.: The Distribution of CO_2 on Mars: A Spectroscopic Determination of Surface Topography. ICARUS 15, 1971, p. 204-232.

28. Parkinson, T. D.; and Hunten, D. M.: CO_2 Distribution on Mars. ICARUS 18, 1973, pp. 29-53.

29. Kliore, A. J.; et al.: The Atmosphere of Mars from Mariner 9 Radio Occultation Measurements. ICARUS 17, 1972, pp. 484-516.

30. Masursky, H.; et al.: Mariner 9 TV Reconnaissance of Mars and Its Satellites: Preliminary Results. Science 175, 1972, pp. 294-304.

31. Sagan, C.; and Pollack, J. B.: Elevation Differences on Mars. J. G. R., Vol. 73, 1968, pp. 1373-1387.

32. Binder, A. B.: Topography and Surface Features of Mars. ICARUS, Vol. 11, 1969, pp. 24-35.

33. Pettengill, G. H.; et al.: Radar Measurements of Martian Topography. Astronautics Journal 74, 1969, pp. 461-482.

34. Counselman, C. C.: Observations of Mars from Earth Between 1965 and 1969. ICARUS 18, 1973, pp. 1-7.

35. Downs, G. S.; et al.: Martian Topography and Surface Properties as Seen by Radar: The 1971 Opposition. ICARUS 18, 1973, pp. 8-21.

36. Pettengill, G. H.; Shapiro, I. I.; and Rogers, A. E. E.: Topography and Radar Scattering Properties of Mars. ICARUS 18, 1973, pp. 22-28.

37. Hanel, R.; et al.: Investigation of the Martian Environment by Infrared Spectroscopy on Mariner 9. ICARUS 17, 1972, pp. 423-442.

38. Cain, D. L.; et al.: The Shape of Mars from the Mariner 9 Occultations. ICARUS 17, 1972, pp. 517-524.

39. Dollfus, A.: New Optical Measurements of Planetary Diameters – Part IV: Planet Mars. ICARUS 17, 1972, pp. 525-539.

40. McElroy, M. B.: Atomic and Molecular Processes in the Martian Atmosphere. Advances in Atomic and Molecular Physics, Vol. 9, Academic Press (New York), 1973, pp. 323-363.

41. Owen, T. C.: The Composition and Surface Pressure of the Martian Atmosphere Results from the 1965 Opposition. Astrophysics Journal, Vol. 146, 1966, pp. 257-270.

42. Spinrad, H.; et al.: High-Dispersion Spectroscopic Observations of Mars; I. The CO_2 Content and Surface Pressure. Astrophysics Journal, Vol. 146, 1966, pp. 331-338.

43. Belton, M. J. S.; Broadfoot, A. L.; and Hunten, D. M.: Abundance and Temperature of CO_2 on Mars During the 1967 Opposition. J. G. R., Vol. 73, No. 15, 1968, pp 4795-4806.

44. Giver, L. P.; et al.: The Martian CO_2 Abundance from Measurements in the 1.05μ Band. Ap. J., Vol. 153, No. 1, 1968, pp. 285-289.

45. Carleton, N. P.; et al.: Measurement of the Abundance of CO_2 in the Martian Atmosphere. Ap. J., Vol. 155, No. 1, 1969, pp. 323-331.

46. Young, L. D. G.: Interpretation of High Resolution Spectra of Mars. I. CO_2 Abundance and Surface Pressure Derived from the Curve of Growth. ICARUS, Vol. 11, No. 3, 1969, pp. 386-389.

47. Goody, R.: The Atmospheres of Mars and Venus. Naturwissenschaften, Vol. 57, No. 1, 1970, pp. 10-16.

48. Dalgarno, A.; and McElroy, M. B.: Mars: Is Nitrogen Present? Science, 170, 1970, pp. 167-168.

49. Kaplan, L. D.; Connes, J.; and Connes, P.: Carbon Monoxide in the Martian Atmosphere. Ap. J., Vol. 157, No. 3, 1969, pp. L187-192.

50. Anon.: Mariner-Mars 1969 A Preliminary Report. NASA SP-225, 1969.

51. Herr, K. C.; et al.: Martian Topography from the Mariner 6 and 7 Infrared Spectra. Astronautics Journal, Vol. 75, No. 8, 1970, pp. 883-894.

52. Steinbacher, R. H.; et al.: Mariner 9 Science Experiments: Preliminary Results. Science, Vol. 75, January 21, 1972, pp. 293-294.

53. Spinrad, H.; Munch, G.; and Kaplan, L. D.: The Detection of Water Vapor on Mars. Astrophysical Journal, Vol. 137, 1963, pp. 1319-1321.

54. Dollfus, A.: Physique Planetaire Analyse des Mesures de la quantite de Vapeur d'eau dans l'atmosphere de la planete Mars. Academy of Science, Paris, Vol. 261, No. 5, 1965, pp. 1603-1606.

55. Schorn, R. A.; et al.: High-Dispersion Spectroscopic Observations of Mars: II. The Water Vapor Variations. Astrophysical Journal, Vol. 147, 1967, pp. 743-752.

56. Schorn, R. A.; Farmer, C. B.; and Little, S. J.: High Dispersion Spectroscopic Studies of Mars: III. Preliminary Results of 1968-1969 Water Vapor Studies. ICARUS, Vol. 11, No. 3, 1969, pp. 283-288.

57. Tull, R. G.: High-Dispersion Spectroscopic Observations of Mars. IV. The Latitudinal Distribution of Atmospheric Water Vapor. ICARUS, Vol. 13, No. 1, 1970, pp. 43-57.

58. Barker, E. S.; et al.: Mars: Detection of Atmospheric Water Vapor During the Southern Hemisphere Spring and Summer Season. Science, Vol. 170, 1970, pp. 1308-1310.

59. Tull, R. G.; and Barker, E. S.: Ground-Based Photoelectric Measures of H_2O on Mars During the Mariner 9 Encounter. Presented at the 2nd Annual Meeting of Division of Planetary Sciences, American Astronomical Society (Kona, Hawaii), March 1972.

60. Moroz, V. I.; and Ksanfomaliti, L. V.: Preliminary Results of the Astrophysical Observations of Mars from AIS Mars-3. Presented at URSI/IAU/COSPAR Symposium on Planetary Atmospheres and Surfaces (Madrid, Spain), May 10-13, 1972.

61. Leovy, C. B.; et al.: The Martian Atmosphere: Mariner 9 Television Experiment Progress Report. ICARUS 17, 1972, pp. 373-393.

62. Morrison, D.; Sagan, C.; and Pollack, J. B.: Martian Temperatures and Thermal Properties. ICARUS 11, 1969, pp. 36-45.

63. Neugebauer, G.; et al.: Mariner 1969 Infrared Radiometer Results: Temperatures and Thermal Properties of the Martian Surface. Astronautics Journal, 76, 1971, pp. 719-727.

64. Houck, J.R.; et al.: High Altitude Aircraft Infrared Spectroscopic Evidence for Bound Water on Mars. ICARUS 18, No. 3, March 1973, pp. 470-480.

65. Conel, J. E.: Infrared Emissivities of Silicates: Experimental Results and a Cloudy Atmosphere Model of Spectral Emission from Condensed Particulate Mediums. Journal of Geophysics Research, 74, 1969, pp. 1614-1634.

66. Carleton, N.P.; and Traub, W.A.: Detection of Molecular Oxygen on Mars. Science, Vol. 177, 1972, p. 988.

67. Lane, A. L.; et al.: Mariner 9 Ultraviolet Spectrometer Experiment: Observations of Ozone on Mars. ICARUS, Vol. 18, 1973, pp. 102-108.

68. Barth, C. A.; and Hord, C. W.: Mariner 6 and 7 Ultraviolet Spectrometer Results: Topography and Polar Cap. Science, Vol. 17, 1971, pp. 197-201.

69. McElroy, M. B.; and Donahue, T. M.: Stability of Martian Atmosphere. Science, Vol. 177, 1972, pp. 986-988.

70. Spencer, D. F.: Our Present Knowledge of the Martian Atmosphere. AIAA/AAS Stepping Stones to Mars Meeting, Baltimore, Maryland, March 1966.

71. Hess, D. S.; and Pounder, E.: Voyager Environmental Predictions Document. SE003BB001-IB28, NASA JPL, October 1966.

72. House, F. B.: The Seasonal Climatology of Mars. Contribution to Planetary Meteorology, GCA Technical Report No. 66-8-N, March 1966.

73. Ohring, G.; and Mariano, J.: Seasonal and Latitudinal Variations of the Average Surface Temperature Profile of Mars. GCA Technical Report 67-5-N, March 1967.

74. Leovy, C.: Radiative-Convective Equilibrium Calculations for a Two-Layer Mars Atmospheres. Rand Memo, RM-5017, 1966.

75. Gierasch, P.; and Goody, R.: The Effect of Dust on the Temperature of the Martian Atmosphere. Journal of Atmospheric Sciences, 29, 1972, pp. 400-402.

76. Chamberlain, J. W.; and McElroy, M. B.: Martian Atmosphere: The Mariner IV Occultation Experiment. Science, Vol. 152, No. 3718, 1966, pp. 21-25.

77. Smith, N.; and Beutler, A.: A Model Martian Atmosphere and Ionosphere. Report 66-3, University of Michigan, Ann Arbor, Michigan, 1966.

78. Kliore, A. J.; et al.: Mariner 9 S-Band Martian Occultation Experiment: Initial Results on the Atmosphere and Topography of Mars. Science, Vol. 175, January 21, 1972, pp. 313-317.

79. Lou, Y. S.; and Hung, F. T.: A Method for the Prediction of the Martian Temperature and Some Applications of Meteorological Analysis. Proceedings, Third National Conference on Aerospace Meteorology, American Meteorological Society, 1968, pp. 237-246.

80. Lou, Y. S.; et al.: Martian Predictions. Science, Vol. 165, No. 3890, 1969, p. 234.

81. Hess, S. L.: Some Aspects of the Meteorology of Mars. Journal of Meteorology, Vol. 7, 1950, pp. 1-13.

82. Kuiper, G. P.: Visual Observations of Mars, 1956. Ap. J., Vol. 156, 1957, pp. 307-317.

83. Golitsyn, G. S.: On the Martian Dust Storms. ICARUS, 18, 1973, pp. 113-119.

84. Sagan, C.: Sandstorms and Eolian Erosion on Mars. Chapter XII of Mariner Mars 1971 Project Final Report: Vol. IV (ref. 9), July 15, 1973, pp. 171-178.

85. Pirraglia, J. A.; and Conrath, B. J.: Martian Tidal Pressure and Wind Fields Obtained from the Mariner 9 Infrared Spectroscopy Experiment. J. of Atmos. Sci., Vol. 3, No. 2, March 1974, pp. 318-329.

86. Tang, W.: Some Aspects of the Atmospheric Circulation on Mars. NASA CR-262, 1965.

87. Leovy, C. B.; and Mintz, Y.: Numerical Simulation of the General Atmospheric Circulation and Climate on Mars. Journal of Atmospheric Science, Vol. 26, No. 6, 1969, pp. 1167-1190.

88. Gierasch, P.; and Goody, R.: A Study of the Thermal and Dynamical Structure of the Martian Lower Atmosphere. Planetary Space Sciences, Vol. 16, No. 5, 1968, pp. 615-646.

89. Chapman, S.; and Lindzen, R. S.: Atmospheric Tides. Reidel Publishing Co., (Dordrecht, Holland), 1970.

90. Lindzen, R. S.: The Application and Applicability of Terrestrial Atmospheric Tidal Theory to Venus and Mars. Journal of Atmospheric Science, Vol. 27, July 1970, pp. 536-549.

91. Gierasch, P.; and Sagan, C.: A Preliminary Assessment of Martian Wind Regimes. ICARUS 14, 1970, pp. 312-318.

92. Blumsack, S. L.; Gierasch, P. J.; and Wessel, W. R.: An Analytical and Numerical Study of the Martian Planetary Boundary Layer over Slopes. Journal of Atmospheric Science, Vol. 30, 1972, pp. 66-82.

93. Blumsack, S. L.; and Gierasch, P. J.: The Vertical Thermal Structure of the Martian Atmosphere: Modifications by Motions. ICARUS 18, 1973, pp. 126-133.

94. Henry, R. M.: Wind and Gust Design Criteria for the Martian Atmosphere. Proceedings, Third National Conference on Aerospace Meteorology (New Orleans, Louisiana), 1968, pp. 356-360.

95. Dessler, A. J.: Ionizing Plasma Flux in the Martian Upper Atmosphere. In the Atmospheres of Venus and Mars, Gordon and Breach Science Publishers, Inc. (New York), 1968, pp. 241-250.

96. Fjeldbo, G.; Kliore, A.; and Seidel, B.: The Mariner 1969 Occultation Measurements of the Upper Atmosphere of Mars. Radio Science, Vol. 5, 1970, pp. 381-386.

97. Fehsenfeld, F. C.; Dunkin, D. B.; and Ferguson, E. E.: Rate Constants for the Reaction of CO_2^+ with O, O_2 and NO; N_2^+ with O and NO; and O_2^+ with NO. Planetary Space Sciences, Vol. 18, 1970, pp. 1267-1269.

98. Barth, C. A.; et al.: Mariner 9 Spectrometer Experiment: Mars Airglow Spectroscopy and Variations in Lyman Alpha. ICARUS 17, 1972, pp. 457-468.

99. Cloutier, P. A.; McElroy, M. B.; and Michel, F. C.: Modification of the Martian Ionosphere by the Solar Wind. Journal of Geophysical Research, Vol. 74, 1969, pp. 6215-6228.

100. Cloutier, P. A.; and Daniell, R. A., Jr.: Ionospheric Currents Induced by Solar Wind Interaction with Planetary Atmospheres. Planetary Space Sciences, Vol. 21, 1973, pp. 463-474.

101. Bauer, S. J.; and Hartle, R. E.: On the Extent of the Martian Ionosphere. J. of Geophysical Research, Vol. 78, No. 16, June 1, 1973, pp. 3169-3171.

102. Dolginov, Sh. Sh.; Yeroshenko, Ye. G.; and Zhuzgov, L. N.: The Magnetic Field in the Very Close Neighborhood of Mars According to Data from the Mars 2 and Mars 3 Spacecraft. J. of Geophysical Research, Vol. 78, 1973, pp. 4779-4786.

103. Kliore, A. J.; et al.: S-Band Radio Occultation Measurements of the Atmosphere and Topography of Mars with Mariner 9: Extended Mission Coverage of Polar and Intermediate Latitudes. Chapter XXXVI of Mariner Mars 1971 Project Final Report: Vol. IV (ref. 9), July 15, 1973, pp. 473-494.

104. Barth, C. A.; et al.: Mariner 6 and 7 Ultraviolet Spectrometer Experiment: Upper Atmosphere Data. Journal of Geophysical Research, Vol. 76, 1971, pp. 2213-2227.

105. Dementyeva, N. N.; et al.: Preliminary Results of Measurements of UV Emissions Scattered in the Martian Upper Atmosphere. ICARUS, Vol. 17, 1972, pp. 475-483.

106. Anderson, D. E., Jr.; and Hord, C. W.: Mariner 6 and 7 Ultraviolet Spectrometer Experiment: Analysis of Hydrogen Lyman Alpha Data. Journal of Geophysics Research, Vol. 76, 1971, pp. 6666-6673.

107. Strickland, D. J.; Thomas, G. E.; and Sparks, P. R.: Mariner 6 and 7 Ultraviolet Spectrometer Experiment: Analysis of the OI 1304A and 1356A Emission. Journal of Geophysical Research, Vol. 77, 1972, pp. 4052-4068.

108. Stewart, A. I.: Mariner 6 and 7 Ultraviolet Spectrometer Experiment: Implications of CO_2^+, CO, and O Airglow. Journal of Geophysics Research, Vol. 77, 1972, pp. 54-68.

109. Stewart, A. I.; et al.: Mariner 9 Ultraviolet Spectrometer Experiment: Structure of Mars' Upper Atmosphere. ICARUS, Vol. 17, 1972, pp. 469-474.

110. Barker, E. S.: Detection of O_2 in the Martian Atmosphere with the Echelle-Coude Scanner of the 107-inch Telescope. Bull. Amer. Astron. Soc., Vol. 4, 1972, pp. 371, 372.

111. McElroy, M. B.: Ionization Processes in the Atmospheres of Venus and Mars. Ann. Geophy., Vol. 26, No. 2, 1970, pp. 643-652.

112. Stewart, R. W.; and Hogan, J. S.: Solar Cycle Variation of Exospheric Temperatures on Mars and Venus: A Prediction of Mariners 6 and 7. Science, Vol. 175, 1969, pp. 386-388.

113. Smith, S. A.; and Smith, B. A.: Diurnal and Seasonal Behavior of Discrete White Clouds on Mars. ICARUS, Vol. 16, pp. 509-521.

114. Curran, R. J.; et al.: Mars: Mariner 9 Spectroscopic Evidence for H_2O Ice Clouds. Science, Vol. 182, NO. 4110, October 26, 1973, pp. 381-383.

115. Pearl, J.; et al.: Results from the Infrared Spectroscopy Experiment on Mariner 9. Exploration of the Planetary System, Proceedings of IAU Symposium 65, A. Woszczyk and C. Iwaniszewska, eds., D. Reidel (Dordrecht, Holland), 1974, p. 201.

116. Briggs, G. A.; and Leovy, C. B.: Mariner 9 Observations of the Mars North Polar Hood. Bulletin of the American Meterological Society, Vol. 55, No. 4, April 1974, pp. 278-296.

117. Leovy, C. B.; et al.: Mariner Mars 1969: Atmospheric Results. Journal of Geophysical Research, Vol. 76, 1971, pp. 297-312.

118. Herr, K. C.; and Pimentel, G.: Evidence for Solid Carbon Dioxide in the Upper Atmosphere of Mars. Science, Vol. 167, 1970, pp. 47-49.

119. Smith, R. E., editor: Space and Planetary Environment Criteria Guidelines for Use in Space Vehicle Development (1971 Revision). NASA TM-X-64627, November 15, 1971.

120. Jordan, J. F.; and Lovell, J.: Mariner 9, An Instrument of Dynamical Science. Presented at AAS/AIAA Astrodynamics Conference (Vail, Colo.), July 16-18, 1973.

121. Pitts, D.: A Computer Program for Calculating Model Planetary Atmospheres. NASA TN D-4292, 1968.

122. Strickland, D. J.; et al.: Mariner 9 Ultraviolet Spectrometer Experiment: Mars Atomic Oxygen 1304-A Emission. Chapter XXIII of Mariner Mars 1971 Project Final Report: Vol. IV (ref. 9), July 15, 1973, pp. 355-368.

123. Conrath, B.; et al.: Atmospheric and Surface Properties of Mars Obtained by Infrared Spectroscopy on Mariner 9. Chapter XX of Mariner Mars 1971 Project Final Report: Vol. IV (ref. 9), July 15, 1973, pp. 299-314.

124. Anon.: Mariner 9 Infrared Interferometer Spectrometer (IRIS) Reduced Data Records Documentation. NASA X-622-73-305, Goddard Space Flight Center, October 1973.

NASA SPACE VEHICLE DESIGN CRITERIA MONOGRAPHS

ENVIRONMENT

SP-8005	Solar Electromagnetic Radiation, revised May 1971
SP-8010	Models of Mars' Atmosphere (1974), revised December 1974
SP-8011	Models of Venus Atmosphere (1972), revised September 1972
SP-8013	Meteoroid Environment Model 1969 (Near Earth to Lunar Surface), March 1969
SP-8017	Magnetic Fields Earth and Extraterrestrial, March 1969
SP-8020	Mars Surface Models (1968), May 1969
SP-8021	Models of Earth's Atmosphere (90 to 2500 km), revised March 1973
SP-8023	Lunar Surface Models, May 1969
SP-8037	Assessment and Control of Spacecraft Magnetic Fields, September 1970
SP-8038	Meteoroid Environment Model 1970 (Interplanetary and Planetary), October 1970
SP-8049	The Earth's Ionosphere, March 1971
SP-8067	Earth Albedo and Emitted Radiation, July 1971
SP-8069	The Planet Jupiter (1970), December 1971
SP-8084	Surface Atmospheric Extremes (Launch and Transportation Areas), revised June 1974
SP-8085	The Planet Mercury (1971), March 1972
SP-8091	The Planet Saturn (1970), June 1972
SP-8092	Assessment and Control of Spacecraft Electromagnetic Interference, June 1972

SP-8103 The Planets Uranus, Neptune, and Pluto (1971), November 1972

SP-8105 Spacecraft Thermal Control, May 1973

SP-8111 Assessment and Control of Electrostatic Charges, May 1974

STRUCTURES

SP-9011 Buffeting During Atmospheric Ascent, revised November 1970

SP-8002 Flight-Loads Measurements During Launch and Exit, revised June 1972

SP-8003 Flutter, Buzz, and Divergence, July 1964

SP-8004 Panel Flutter, revised June 1972

SP-8006 Local Steady Aerodynamic Loads During Launch and Exit, May 1965

SP-8007 Buckling of Thin-Walled Circular Cyclinders, revised August 1968

SP-8008 Prelaunch Ground Wind Loads, November 1965

SP-8009 Propellant Slosh Loads, August 1968

SP-8012 Natural Vibration Modal Analysis, September 1968

SP-8014 Entry Thermal Protection, August 1968

SP-8019 Buckling of Thin-Walled Truncated Cones, September 1968

SP-8022 Staging Loads, February 1969

SP-8029 Aerodynamic and Rocket-Exhaust Heating During Launch and Ascent, May 1969

SP-8031 Slosh Suppression, May 1969

SP-8032 Buckling of Thin-Walled Doubly Curved Shells, August 1969

SP-8035 Wind Loads During Ascent, June 1970

SP-8040 Fracture Control of Metallic Pressure Vessels, May 1970

SP-8042 Meteoroid Damage Assessment, May 1970

SP-8043	Design Development Testing, May 1970
SP-8044	Qualification Testing, May 1970
SP-8045	Acceptance Testing, April 1970
SP-8046	Landing Impact Attenuation for Non-Surface-Planning Landers, April 1970
SP-8050	Structural Vibration Prediction, June 1970
SP-8053	Nuclear and Space Radiation Effects on Materials, June 1970
SP-8054	Space Radiation Protection, June 1970
SP-8055	Prevention of Coupled Structure-Propulsion Instability (Pogo), October 1970
SP-8056	Flight Separation Mechanisms, October 1970
SP-8057	Structural Design Criteria Applicable to a Space Shuttle, revised March 1972
SP-8060	Compartment Venting, November 1970
SP-8061	Interaction with Umbilicals and Launch Stand, August 1970
SP-8062	Entry Gasdynamic Heating, January 1971
SP-8063	Lubrication, Friction, and Wear, June 1971
SP-8066	Deployable Aerodynamic Deceleration Systems, June 1971
SP-8068	Buckling Strength of Structural Plates, June 1971
SP-8072	Acoustic Loads Generated by the Propulsion System, June 1971
SP-8077	Transportation and Handling Loads, September 1971
SP-8079	Structural Interaction with Control Systems, November 1971
SP-8082	Stress-Corrosion Cracking in Metals, August 1971
SP-8083	Discontinuity in Metallic Pressure Vessels, November 1971
SP-8095	Preliminary Criteria for the Fracture Control of Space Shuttle Structures, June 1971

SP-8099 Combining Ascent Loads, May 1972

GUIDANCE AND CONTROL

SP-8015 Guidance and Navigation for Entry Vehicles, November 1968

SP-8016 Effects of Structural Flexibility on Spacecraft Control Systems, April 1969

SP-8018 Spacecraft Magnetic Torques, March 1969

SP-8024 Spacecraft Gravitational Torques, May 1969

SP-8026 Spacecraft Star Trackers, July 1970

SP-8027 Spacecraft Radiation Torques, October 1969

SP-8028 Entry Vehicle Control, November 1969

SP-8033 Spacecraft Earth Horizon Sensors, December 1969

SP-8034 Spacecraft Mass Expulsion Torques, December 1969

SP-8036 Effects of Structural Flexibility on Launch Vehicle Control Systems, February 1970

SP-8047 Spacecraft Sun Sensors, June 1970

SP-8058 Spacecraft Aerodynamic Torques, January 1971

SP-8059 Spacecraft Attitude Control During Thrusting Maneuvers, February 1971

SP-8065 Tubular Spacecraft Booms (Extendible, Reel Stored), February 1971

SP-8070 Spaceborne Digital Computer Systems, March 1971

SP-8071 Passive Gravity-Gradient Libration Dampers, February 1971

SP-8074 Spacecraft Solar Cell Arrays, May 1971

SP-8078 Spaceborne Electronic Imaging Systems, June 1971

SP-8086 Space Vehicle Displays Design Criteria, March 1972

SP-8096 Space Vehicle Gyroscope Sensor Applications, October 1972

SP-8098 Effects of Structural Flexibility on Entry Vehicle Control Systems, June 1972

SP-8102 Space Vehicle Accelerometer Applications, December 1972

CHEMICAL PROPULSION

SP-8025 Solid Rocket Motor Metal Cases, April 1970

SP-8039 Solid Rocket Motor Performance Analysis and Prediction, May 1971

SP-8041 Captive-Fired Testing of Solid Rocket Motors, March 1971

SP-8048 Liquid Rocket Engine Turbopump Bearings, March 1971

SP-8051 Solid Rocket Motor Igniters, March 1971

SP-8052 Liquid Rocket Engine Turbopump Inducers, May 1971

SP-8064 Solid Propellant Selection and Characterization, June 1971

SP-8073 Solid Propellant Grain Structural Integrity Analysis, June 1973

SP-8075 Solid Propellant Processing Factors in Rocket Motor Design, October 1971

SP-8076 Solid Propellant Grain Design and Internal Ballistics, March 1972

SP-8080 Liquid Rocket Pressure Regulators, Relief Valves, Check Valves, Burst Disks, and Explosive Valves, March 1973

SP-8081 Liquid Propellant Gas Generators, March 1972

SP-8087 Liquid Rocket Engine Fluid-Cooled Combustion Chambers, April 1972

SP-8088 Liquid Rocket Metal Tanks and Tank Components, May 1974

SP-8090 Liquid Rocket Actuators and Operators, May 1973

SP-8094 Liquid Rocket Valve Components, August 1973

SP-8097 Liquid Rocket Valve Assemblies, November 1973

SP-8100 Liquid Rocket Engine Turbopump Gears, March 1974

SP-8101 Liquid Rocket Engine Turbopump Shafts and Couplings, September 1972

SP-8110 Liquid Rocket Engine Turbines, January 1974

NASA-Langley, 1975

NATIONAL AERONAUTICS AND SPACE ADMINISTRATION
WASHINGTON, D.C. 20546

OFFICIAL BUSINESS
PENALTY FOR PRIVATE USE $300

SPECIAL FOURTH-CLASS RATE BOOK

POSTAGE AND FEES PAID
NATIONAL AERONAUTICS AND
SPACE ADMINISTRATION
451

POSTMASTER · If Undeliverable (Section 158 Postal Manual) Do Not Return